Published in final edited form as:
J Aerosol Sci. 2022 January ; 159: 1–31. doi:10.1016/j.jaerosci.2021.105881.

Particle emissions from mobile sources: Discussion of ultrafine particle emissions and definition

David Kittelson[a], **Imad Khalek**[b], **Joseph McDonald**[c], **Jeffrey Stevens**[c], **Robert Giannelli**[c,*]

[a]University of Minnesota, Department of Mechanical Engineering, Minneapolis, MN, 55455, USA

[b]Southwest Research Institute, Powertrain Engineering Division, San Antonio, TX, 78238, USA

[c]U. S. Environmental Protection Agency, Office of Transportation and Air Quality, National Vehicle and Fuel Emissions Laboratory, Ann Arbor, MI, 48105, USA

Abstract

There is no universally agreed upon definition for ultrafine particles (UFP). Commonly used definitions for UFP are either particle number below 100 nm or total particle number, but without an agreed upon lower cut point. For example, a lower cut point of 3 nm compared to 10 nm could result in a substantially higher count. Another definition for UFP is total particle mass but without a commonly agreed upon aerodynamic diameter upper cut point, e.g., below 100 nm, 200 nm, 300 nm, etc. Yet another definition is lung deposited surface area weighted by lung deposition fraction, found mainly in the particle mobility diameter range from 20 to 400 nm. It is clear from these definitions that there are inconsistencies in the way UFP is used and defined in the literature. Sometimes these metrics are well correlated, sometimes not.

In this paper we suggest three exposure metrics: UFP-N, UFP-M, and UFP-S, that we believe will add clarity. These metrics represent total number, mass, and surface area below 500 nm, respectively. For surface area and mass, the 500 nm cut point can be either aerodynamic or mobility diameter depending upon measurement methodology. For all metrics, this cut point captures nearly all of the primary particle emissions from mobile sources. Furthermore, UFP-N would include a lower cut point of 3–6 nm and would not require an upper size cut point because there is very little particle number above 500 nm or even above 100 nm. Thus, our definition of UFP-N is consistent with the current definition of ultrafine number except for, importantly, the specification of a lower cut point. These exposure metrics can help facilitate consistency in the characterization of both short- and long-term UFP ambient exposures and associated health effects in epidemiological studies.

*Corresponding author. giannelli.bob@epa.gov (R. Giannelli).

Declaration of competing interest

The authors declare that they have no known competing financial interests or personal relationships that could have appeared to influence the work reported in this paper.

Keywords

Ultrafine particulate matter; Mobile source particulate matter emissions; Particulate matter sampling; Particulate matter measurement

1. Introduction

Exposure to primary and secondary airborne ultrafine particles (UFP) may have negative impacts on human health (U.S. EPA, 2019; Schraufnagel, 2020), and may disproportionately impact low income and minority communities due to their proximity to UFP sources (Brugge et al., 2015). However, some of the uncertainties and research needs identified in EPA's 2009 p.m. Integrated Science Assessment (ISA) (U.S. EPA, 2009) regarding the lack of a standardized UFP definition and standard reference measurements have led to uncertainties in epidemiological studies that remain unresolved and continue to be articulated in EPA's 2019 p.m. ISA (U.S. EPA, 2019). Additionally, measurement metrics (e.g. exposure indicator for epidemiological studies) and definitions of UFP are not standardized, which makes the comparison and interpretation of results across health studies challenging.

The degree to which specific anthropogenic emission sources contribute to the overall burden of UFP at any location and time is highly variable and depends on the size distribution and composition of particles emitted from that source as well as the state of the atmosphere and its composition. The lack of a standardized ambient or source reference method for UFP has been identified (U.S. EPA, 2009; Baldauf et al., 2016; U.S. EPA, 2019) as a critical ongoing source of uncertainty that creates serious challenges for developing emissions inventories and for understanding potential health or environmental impacts.

In this paper, using a selection of representative papers, we examine the UFP definition and how primary UFP have been sampled from mobile sources under on-road, near-road, and laboratory conditions, and will recommend new UFP metrics for ambient and laboratory health studies along with suggestions for tailpipe sampling and measurement of UFP. An ongoing question about UFP is whether its effects are already captured by $PM_{2.5}$, due to $PM_{2.5}$ representing a distribution of particles that encompasses the UFP size range. We will argue that the well-established association between $PM_{2.5}$ and adverse health effects, mainly based on area wide (scale several km) exposures and including secondary aerosol formation, is facilitated by the clear definition of $PM_{2.5}$. On the other hand, the lack of clear definition of UFP makes it difficult to compare results across epidemiological studies, especially for near source exposures (scale 100–300 m).

In this paper, we are addressing total UFP that includes solid and semi-volatile particles. The European Union (EU) has adopted a system for measuring solid particle number for regulation of mobile sources (Giechaskiel, 2012; Lähde & Giechaskiel, 2021; Samaras et al., 2020). The EU method was designed to regulate source emissions and is not an appropriate indicator of on-road and near road ambient exposures because it excludes semi-volatile material, an important fraction of ambient aerosols. Solid particle number has not been adopted by the U.S. EPA for mobile source standards in the United States.

2. UFP definition and overview

UFP are typically defined operationally as particulate matter[1] with a particle diameter (D_p) of 100 nm or less (Health Effects Institute, 2013; U.S. EPA, 2019). There is still ongoing debate regarding a definition for UFP with respect to the classification methods, the particle size upper and lower cut points, and the measured properties (e.g., number, surface area, mass) (Baldauf et al., 2016). There is currently no EPA reference method for either ambient or source measurement of UFP, however, the EPA is currently accepting UFP data into EPA's Air Quality System (U.S. EPA, n.d.) from state agencies. The ambiguity surrounding a precise definition of UFP has resulted in a variety of UFP classification and measurement methods within published literature. Lack of standardized reference methods are a significant factor in the uncertainty surrounding epidemiological and laboratory studies of the human health effects of UFP (U.S. EPA, 2019; Health Effects Institute, 2013; U.S. EPA, 2009).

In 1974, Shanty investigated human respiratory deposition of UFP using an 80 nm monodisperse test aerosol (Shanty, 1974). Blanchard and Willeke (1983) defined UFP as having a diameter equal to or less than 200 nm. The popular UFP description of sub-100 nm diameter particle number was referenced within early work on engineered nanostructure materials by Sumio Iijima and subsequent studies by Günter Oberdörster et al. on UFP toxicity (Ferin et al., 1990; Iijima, 1984, 1985; Oberdörster et al., 1990a, 1995; Oberdörster & Yu, 1990b). Oberdörster's rodent inhalation studies suggested that fresh sub-50 nm aerosols have higher acute toxicity than aged, agglomerated aerosols of larger particle size (≥250 nm). Studies continued in the 1990's through the early 2000's, which identified particle size, particle surface area and surface chemistry (especially oxidative stress activity), charge, crystallinity, coating, and biopersistence as key dosimetric parameters impacting UFP toxicity in mammals and humans (Oberdörster et al., 2007).

UFP consist of heterogeneously and homogeneously nucleated particles, solid aggregate structures of carbon as well as trace metal compounds containing from one to several hundred individual particles along with adsorbed and absorbed semi-volatile and volatile compounds (Cass et al., 2000; Donaldson et al., 2001; Harrison et al., 2000). Near roadway, the aerosol is dominated by engine exhaust (Jacobson et al., 2005; Nanzetta & Holmén, 2004; Rönkkö & Timonen, 2019; Saha et al., 2018; Zhang et al., 2004; Zhang & Wexler, 2004). UFP and nanoparticles or Aitken nuclei ($D_p \leq 50$ nm) are part of a continuum of particle size definitions that include U.S. EPA regulatory definitions for PM_{10} ($D_p \leq 10$ μm) (U.S. CFR, 2020a) and fine particles or $PM_{2.5}$ ($D_p \leq 2.5$ μm) (U.S. CFR, 2020b), but unlike PM_{10} and $PM_{2.5}$ there is not a regulatory definition for UFP.

The origins of these size-dependent definitions were heavily influenced by the Whitby model of ambient particle size distribution (Whitby, 1967; Clark & Whitby, 1967; Whitby et al., 1972; Husar & Whitby, 1973; Willeke & Whitby, 1975; Cantrell & Whitby, 1978; Whitby & Sverdrup, 1980; Vogt et al., 2003; Nanzetta & Holmén, 2004; Ban-Weiss et al.,

[1]Particulate Matter from mobile sources is defined as materials that consist of carbonaceous aggregates (soot), ash, organic carbon and inorganic materials.

2010; Paasonen et al., 2016; Saha et al., 2018). This body of work found that both ambient particulate matter and many sources of ambient particle emissions could be reasonably modeled as aerosols within three,[2] approximately log-normal, overlapping size distributions. The three overlapping size distributions (nucleation, accumulation, and coarse modes) are discussed in further detail below. The Whitby model has been extended to include laboratory measurements of mobile-source aerosols and on and near roadway ambient aerosols (Abdul-Khalek et al., 1998; Burtsher, 2005; Johnson et al., 2005; Keskinen & Rönkkö, 2010; Kittelson, 1998; Kittelson et al., 2006a, 2006b; Kittelson & Kraft, 2015).

Near-roadway ambient aerosols result from mixing particles and gases formed in the engine with ambient air. This process, illustrated in Figs. 2–1, is complex and results in gas to particle conversion of semi-volatile materials present in mobile source exhaust as it is diluted and cooled by ambient air.

Fig. 2–2 shows the history of near-roadway particle evolution from the onset of formation within the engine cylinder to the ambient aerosol that exists over a roadway. It highlights some of the chemical and physical processes that impact how the ambient aerosol size distribution changes over a relatively short time span (~0–2 s from source of emission) (Kittelson, Watts, & Johnson, 2006; Rönkkö & Timonen, 2019). Particles formed during exhaust dilution and cooling are usually considered primary (or delayed primary) particles even though they are not formed in the engine. After this initial rapid dilution and cooling, dilution continues along with aerosol transformations associated with coagulation and partitioning between the gas and particle phases. At the same time secondary organic and inorganic aerosol formation (SOA and SIA) begins.

These processes typically result in approximately lognormal, trimodal size distributions like those shown Figs. 2–3. These size distributions are normalized (to the total or integrated, respective, concentration, C_{total}) particle mobility size distributions for particle number, surface area, lung deposited surface area (LDSA) (Wilson et al., 2007; Fierz et al., 2011; Schmid & Stoeger, 2016; Fissan et al., 2007), and mass. They are representative of a pre-2007 diesel aerosol. Other engine technologies produce aerosols with a similar modal structure although modal size boundaries and concentrations within the modes differ. Figs. 2–3 also contrasts particle size-dependent regulatory definitions, $PM_{2.5}$ and PM_{10} (mass measurements with size cutoff based on aerodynamic diameter), with conventionally used, but not regulatorily defined, definitions of nanoparticles and UFP (metric unspecified but often based on particle number with size cutoff based on mobility diameter).

Models of particle deposition within the human respiratory tract developed in the 1980's and 1990's have influenced categorization of particles by size (International Commission on Radiological Protection, 1994). Particle size is not static upon inhalation. Particle growth, for example, occurs within the human respiratory system by both condensation and adsorption of water vapor and by particle agglomeration. Human respiratory models typically account for such effects. The black line in Figs. 2–3 shows the probability of particle deposition within the respiratory system relative to aerodynamic diameter. The

[2]Sometimes there are additional sub modes associated with multiple vehicle operating conditions.

probability of total respiratory deposition increases as particle size decreases below about 400 nm largely due to increased Brownian diffusion with decreasing particle size. Sub-400 nm aerodynamic diameter particles are thus associated with an increasing probability of thoracic (alveolar, bronchial, tracheal, laryngeal) deposition as particle size decreases, with diffusion to tissue surfaces being a significant contributor to respiratory deposition. Sub-400 nm particles also typically contribute more to the total particle surface area of ambient aerosols than aerosols with D_p larger than 400 nm. Particle surface area may be an important metric with respect to free-radical activity, oxidative stress, and pulmonary inflammation (Dick et al., 2003; Donaldson et al., 2001; Donaldson & Stone, 2003; Oberdörster et al., 2007; Schmid & Stoeger, 2016).

The size ranges (e.g. nanoparticles, UFP, $PM_{2.5}$, PM_{10}), names of specific modes (nucleation, accumulation and coarse), important characteristics for UFP and other ambient aerosol size fractions vary within published literature (U.S. EPA, 2004; Solomon, 2012; Kittelson & Kraft, 2015). There also may be considerable overlap between nucleation, accumulation, and coarse mode particles. Note that "PM_{10}", "Coarse PM", and "$PM_{2.5}$ Fine Particles" are based upon U.S. federal regulatory definitions (mass measurements with size cutoff based on aerodynamic diameter) but the sub-100 nm definition of UFP is by current convention (metric unspecified but often based on particle number with size cutoff based on mobility diameter). The engine exhaust or near roadway size distribution shown in Figs. 2–3 is a subset of PM_{10} with somewhat more narrowly defined modes.

It is important to recognize that the engine exhaust aerosol modal structure shown in Figs. 2–3 is associated with formation mechanisms, temperature, composition, and time histories, but not arbitrary size boundaries.[3] These mechanisms and the formation of the three modes are considered below.

Nucleation mode:

Two types of *solid* nucleation mode particles have been observed: metallic ash particles and small clusters of primary carbonaceous particles (Khalek et al., 1998; Rönkkö & Timonen, 2019; Rönkkö et al., 2017; Alanen et al., 2015). Metal and metal-oxide compounds from fuel, lubricating oil and engine wear evaporate as they pass through high temperature regions surrounding burning fuel packets. As the piston moves downward, temperatures and pressures fall, and these gas phase metallic compounds undergo gas to particle conversion to form solid ash particles. If the ratio of soot[4] to ash is high, most of this material will stick to and decorate the soot particles and a separate ash mode will not form. Conversely, if the ash to soot ratio is high, a separate ash nucleation or nanoparticle mode will form. In some cases, primary carbonaceous particles that have escaped aggregation into larger soot particles are also found in the nucleation mode size range.

Semi-volatile nucleation mode particles are formed later. As in-cylinder processes continue, temperature and pressure drop until the exhaust is discharged from the cylinder, flows

[3]As an example, the accumulation or soot mode geometric mean diameters can range from as small as 20 nm for the soot mode emanating from aircraft turbine engines to as large as 80 nm for the soot mode emanating from older diesel engines.
[4]Soot is defined as an aggregate that is dominated by carbonaceous particles with traces of ash, organic and inorganic compounds.

through the exhaust system, and is discharged into the atmosphere where it is quickly diluted and cooled by ambient air. It is during this dilution and cooling process that semi-volatile materials undergo gas to particle conversion. These particles are usually considered as primary because they form immediately upon dilution of the exhaust plume, but sometimes are called delayed primary (Rönkkö & Timonen, 2019; Rönkkö et al., 2017) or even secondary (Morawska et al., 2008). This is where most of the semi-volatile nucleation mode particles form, and typically most of the nucleation mode particles near roadways are semi-volatile. Just as in the case of ash, soot plays an important role. If the ratio of soot (from both the engine and ambient air) to semi-volatile material is high, the soot scavenges semi-volatile material and suppresses nucleation mode formation. Conversely, if the ratio is low, nucleation mode formation is favored.

Accumulation mode:

The accumulation mode, or soot accumulation mode, sometimes called the soot mode, consists mainly of carbonaceous aggregates formed early in the combustion process in hot, fuel rich regions of the cylinder (Harris & Maricq, 2001; Kittelson, 1998; Morawska et al., 2008). These aggregates consist of dozens to hundreds of primary particles formed by gas to particle conversion of hydrocarbon fragments and grow by coagulation and surface growth to form stable layered or lamellae structures. The soot accumulation mode is typical of engine out conditions for diesel, GDI, and even aircraft gas turbines. However, for some low soot operating conditions, for example diesel engines at very light load (Kittelson et al., 2005) or combustion systems, for example low temperature combustion (Bullock and Olfert, 2014), nucleation and growth of semi-volatile materials cause the nucleation mode to grow into the accumulation mode size range to form a single mode (Khalek, 2006c).

Coarse mode:

The third mode, usually called the coarse mode, consists mainly of mechanically generated particles, e.g., soot re-entrained from in-cylinder and exhaust system surfaces that are discharged with the exhaust, and crankcase fumes as well as roadside particles associated with brake[5] and tire wear (Harrison et al., 2000; Tatli & Clark, 2008; Johnson et al., 2011; Uy et al., 2016). Crankcase fumes are mainly oil droplets atomized from piston rings or oil seals. In older engines they are vented directly into the atmosphere, but many modern engine designs either recycle them into the engine inlet (closed crankcase) and/or capture them in a crankcase filtration system. It should also be noted that at least currently in the U.S. many heavy-duty vehicles vent crankcase fumes directly into the atmosphere. Although, they are treated with a filtration device, it is not as efficient as a typical particle filter.

While the formation mechanisms and chemical composition differ among the three particle size modes, there are also chemical and physical transformations that transport aerosol mass between the modes. Chemical reactions, physical phenomena (agglomeration, condensation, adsorption, absorption, evaporation) and interactions with other processes such as dilution, coagulation and deposition continue as aerosols propagate away from their initial site of

[5]Recent work has shown that particles generated by braking may produce several size modes encompassing the nucleation, accumulation, and coarse ranges (Beji et al., 2020; Farwick zum Hagen et al., 2019).

emission (Rönkkö & Timonen, 2019; Saha et al., 2018; Zhang et al., 2004; Zhang & Wexler, 2004). This further impacts the size distribution, chemical composition, and relative contribution of each mode to ambient UFP concentrations.

As shown in Figs. 2–3, typically, accumulation mode particles are the predominant contributor to UFP mass. Although nucleation mode particles are only a minor contributor to fine particle mass and UFP mass, they are usually a major contributor to particle number. Both nucleation and accumulation mode particles are closely associated with UFP surface area and LDSA.

The position of modes and boundaries between the size distributions depends on the combustion thermochemistry (Kittelson, Watts, Johnson, et al., 2004; Burtscher, 2005; Giechaskiel et al., 2014; Kittelson & Kraft, 2015). Specifically, they can depend on the engine and exhaust system design, operating conditions (e.g., speed and load), ambient air, fuel and lubricant composition (chemical constituents), exhaust aftertreatment, etc. Thus for an older technology diesel engine operating on standard fuel, the modes might be well represented by Figs. 2–3 with a nucleation mode between about 3 and 50 nm, an accumulation mode between about 10 and 500 nm and a coarse mode between about 500 and 2500 nm. It should be noted that the modes overlap and boundaries between the modes shift with operating conditions and fuel. The general modal structure in the submicron region is also observed in particles produced by modern gasoline spark ignition (SI) engines. Figs. 2–4 shows number weighted size distributions from two types of gasoline direct injection (GDI) engines, wall guided and spray guided direct-injection, and from a traditional port fuel injection (PFI) engine (Zhang & McMahon, 2012). All three show distinct nucleation and accumulation modes, although the relative size of the nucleation modes is much smaller than with older technology diesel engines because these engines were equipped with three-way catalysts that largely removed semi-volatile nucleation mode particles. The exhaust aerosol from a modern diesel engine equipped with catalyzed aftertreatment is expected to be dominated by a semi-volatile nucleation mode below about 50 nm (mainly sulfates, in this case produced by the catalyst) and nearly no solid (soot or ash) particles (Khalek et al., 2013). On the other hand, a natural gas fueled SI engine (Khalek et al., 2018), might emit mainly solid nucleation mode particles below about 20 nm and a small soot mode. Clearly rigid boundaries do not apply to the nucleation, accumulation, and coarse size modes.

In the United States it appears likely that most GDI vehicles will be able to meet U.S. Tier 3 standards and California Low Emission Vehicle (LEV) III without particle filters (McDonald, 2021). On the other hand, because of the stringent particle number standards in Europe, essentially all GDI vehicles sold there are equipped with particle filters. In any of these regulatory approaches the standards are extremely tight and future GDI vehicles operating under normal conditions will have very low emissions when operated on regulatory cycles.[6] Similarly, modern diesel engines equipped with catalyzed aftertreatment

[6]We acknowledge however that many GDI and/or PFI vehicles in the U. S. still use commanded enrichment when operating at high load conditions which may result in high particle emissions that are not currently captured on the regulatory cycles (U.S. EPA, 2021). These high off cycle emissions may be similar to older and/or malfunctioning vehicles.

can produce very low emissions although like gasoline vehicles, details of the regulatory approach in the US and EU are different. In this paper, we focus on the size and modal structure of particle emissions from older vehicles.[6] Particle emissions from older and malfunctioning vehicles are likely to continue to be a substantial contributor to roadside exposure to UFP for many years, especially as vehicles with internal combustion engine powertrains transition to all electric drive.

2.1. UFP health effects—In 2009, the U.S. EPA Particulate Matter Integrated Science Assessment (PM-ISA) concluded that health evidence was suggestive of a causal relationship between short-term exposures to UFP[7] and cardiovascular effects, particularly vasomotor function (U.S. EPA, 2009; Baldauf et al., 2016). However, the PM-ISA concluded that data were inadequate to establish a relationship between short-term exposure to UFP and premature mortality or central nervous system effects, or between long-term exposure to UFP and any of the health outcomes evaluated (U.S. EPA, 2009; Baldauf et al., 2016). EPA also recognized that the absence of a national network of UFP monitors to assess ambient concentrations in the U.S. precluded the development of a national inventory of ambient UFP concentrations, including temporal and spatial patterns and trends, and, thus, further limiting information to support UFP epidemiological studies (U.S. EPA, 2011; Baldauf et al., 2016). The EPA concluded that the available scientific information was too limited to provide support for consideration of a distinct standard specifically for UFP at the time of the 2012 p.m. NAAQS review. This is at least partially due to the current imprecise definition of UFP.

In February 2015, the United States Environmental Protection Agency (EPA) sponsored a workshop in Research Triangle Park, NC, USA to review the state of the science on emissions, air quality impacts, and health effects associated with exposures to UFP (Baldauf et al., 2016). In this workshop reports (e.g., Lanzinger et al., 2016; Samet et al., 2007; Su et al., 2015) were given that short-term exposure epidemiological studies provide evidence of an association between exposure to near-roadway UFP and adverse cardiovascular outcomes. However, it is not clear whether such outcomes are more strongly related to UFP or to other particle size ranges and/or co-pollutants (Baldauf et al., 2016). Long-term exposure epidemiological studies are beginning to use modeling approaches to estimate UFP exposures (Saha et al., 2020), but the absence of a universally accepted definition of UFP and the related lack of standardized UFP monitoring networks continue to contribute to uncertainty. Controlled human exposure studies have shown that exposures to UFP (unfortunately defined in many different ways) can result in cardiopulmonary biological changes, but do not yet provide evidence to support the conclusion that UFP are more potent than other PM size fractions (Baldauf et al., 2016). Concerns regarding the translocation of UFP from the lungs into the blood where UFP could impact secondary organs suggest that sub-micron particle size fractions such as UFP may need to be separately considered in assessing the potential adverse effects of PM exposure (Baldauf et al., 2016). Recently, Saha et al. (2020) found that in Pittsburgh, PA, USA $PM_{2.5}$ and UFP were spatially correlated,

[7]The PM-ISA cites studies of UFP using a variety of metrics, including particle mass with inertial classification and particle number with or without size-specific classification.

but not temporally correlated. This further complicates trying to separate epidemiological impacts of UFP and $PM_{2.5}$.

2.2. UFP classification

Particle size (usually diameter) may be determined using a number of different methods, including: electron and optical microscopy, light scattering, inertial separation, diffusion, and electrical mobility. This section will give an abbreviated overview of classification techniques and then a summary of the relationships between particle mobilities and particle diameters (size) which are used in the non-optical classification methods.

Electron microscopy is a fundamental method that can give a great deal of information on size, shape, and composition of particles if coupled with energy dispersion spectroscopy. It can be regarded as a reference method, but it is an offline method that relies on careful sampling and analysis, is expensive and requires specialized equipment and training and thus this method will not be considered further. Optical sizing methods based on light scattering depend on particle size, shape, and refractive index. They are most useful in the size range from about 100 nm–10 μm. Light scattering is very size dependent, varying with the sixth power of diameter, e. g. (Friedlander, 2000), and (van de Hulst, 1957/1981), for particles below approximately 50 nm. This leads to very weak scattering for particle sizes of relevance for UFP measurement. This limits its utility and thus this method will not be considered further.

Another type of optical measurement that gives information on particle size is laser induced incandescence (LII). It relies on heating particles (nearly always elemental carbon) with a short, intense laser pulse and measuring the resulting incandescence. LII of soot was initially proposed and used to measure soot volume fractions and primary particle size, but not size distribution (e.g., Melton, 1984; Roth & Filippov, 1996; Vander Wal et al., 1999; Vander Wal & Weiland, 1994).

The other three particle size measurement methods mentioned are based on inertial separation, diffusion, or electrical mobility, all of which may be applied to UFP measurement (Hinds, 1999). They all depend on the mechanical mobility of a particle.

The mechanical mobility, B, is the ratio of particle velocity to an external, applied force under steady state conditions (e.g., Hinds, 1999). For a spherical particle with velocity, v, experiencing a drag force, f, in a fluid it is defined as:

$$B = \frac{v}{f} = \frac{C_c}{3\pi\eta D_p} \tag{1}$$

where C_c, is the Cunningham slip correction, η is viscosity, and D_p is particle diameter. For non-spherical particles this must be corrected using a dynamic shape factor, χ:

$$B = \frac{C_c}{3\pi\eta D_e \chi} \tag{2}$$

where D_e is the (spherical) volume equivalent diameter.

All inertial separation methods are based on mechanical mobility. The simplest of these methods is gravitational settling where the applied force is gravity. The settling velocity (the speed at which the drag and gravitational forces balance and the net motion is a constant speed), V_s, is given by:

$$V_s = F_g B \tag{3}$$

where F_g is the force of gravity. For a spherical particle:

$$V_s = \frac{\rho_p D_p^2 g C_c}{18\eta} \tag{4}$$

where ρ_p is the particle density and g is the acceleration due to gravity.

The ***aerodynamic diameter*** of a particle is the diameter of a unit density (1 g/cm^3) particle sphere having the same settling velocity as the particle being characterized. The aerodynamic diameter depends upon particle size, shape, and density. The definition is the same if the force is inertial, e.g., produced by acceleration in an inertial field, as in an inertial impactor, instead of a gravitational one.

Another diameter related to mechanical mobility is the diffusion equivalent diameter. The Brownian diffusion coefficient of a particle is related to mobility by:

$$D = kTB \tag{5}$$

where k is Boltzmann's constant and T is temperature. The ***diffusion equivalent diameter*** is the diameter of a spherical particle having the same diffusion coefficient as the particle in question. From the definition of B we see that diffusion diameter depends on particle size and shape, but not density. It is also called the mechanical mobility diameter and the Stokes diameter.

The ***electrical mobility diameter*** is also related to mechanical mobility. The electrical mobility, Z, is defined as the ratio of terminal velocity of a charged particle moving in an electric field to the strength of the field. The electrical mobility is given by:

$$Z = neB \tag{6}$$

where n is the number of elementary charges and e is the charge of an electron. The ***electrical mobility equivalent diameter*** is the diameter of a spherical particle, that when charged to the same level, (usually a single charge) has the same electrical mobility as the particle being characterized. Like the diffusion diameter, *electrical mobility equivalent diameter depends on particle size and shape, but not density*. The relationship between the Stokes, aerodynamic and electrical mobility diameter are discussed in detail by Hinds (1999). It's worth noting if the density of particles is less than 1 g/cm^3 that the aerodynamic is smaller than the mobility diameter.

3. Mobile source emissions of UFP

EPA has not published inventory estimates of UFP but has published inventories of fine particulate ($PM_{2.5}$) emissions (U.S. EPA, 2020, p. 2017). Mobile sources account for approximately 20% of anthropogenic fine particle emissions in the U.S., with a relative contribution of approximately 42% from highway (light-duty and heavy-duty vehicles) sources and approximately 58% from nonhighway (nonroad equipment, locomotives, marine vessels, aircraft) sources (U.S. EPA, 2020, p. 2017). Fine particle emissions in 2017 for major mobile source categories in the U.S. are summarized in Figs. 3–1.

Emissions of UFP from mobile sources include direct tailpipe emissions; formation of secondary aerosols from exhaust emissions; formation of secondary aerosols from fuel system emissions, which may also include refueling, evaporative and running-loss emissions; and aerosols from crankcase fumes, brake, clutch-pack and tire wear. Research on mobile source UFP emissions has focused primarily on direct tailpipe emissions of UFP from diesel and gasoline SI engines and light-duty vehicles as the most significant sources of mobile source UFP.

Direct tailpipe PM emissions from mobile source combustion engines are a complex mixture composed chiefly of:

- Elemental carbon (EC), black carbon (BC) or soot particles formed primarily as pyrolysis products of partially combusted fuel (Birch, 2002; Birch & Cary, 1996; Chow et al., 2001, 2004; Khalek et al., 2011, 2013, 2015)
- Metal oxides, sulfates, phosphates and other metallic and nonmetallic ash compounds, chiefly from lubricating oil additives and engine wear (Khalek et al., 2011, 2013, 2015)
- Semi-volatile compounds that begin primarily in the gas phase and then as the exhaust gases cool are adsorbed and absorb onto other particles or are heterogeneously or homogenously nucleated including (Khalek et al., 2011, 2013, 2015):
  - Semi-volatile organic compounds (SVOC) from the lubricant and fuel
  - Sulfates from sulfur in the fuel and lubricating oil
  - Nitrate compounds.

Gasoline SI and diesel engines in both highway and nonroad applications are also significant sources of complex gas-phase and particle-phase volatile organic compound (VOC) and SVOC emissions. Depending on ambient conditions, SVOC from engine emissions can directly form primary organic aerosols (POA) or VOC can undergo atmospheric oxidation reactions to form secondary organic compounds (SOA) (Gentner et al., 2017). Depending on location, season, and time of day, POA and SOA can be a significant fraction of UFP within U.S. urban airsheds (Daher et al., 2012). Nitrogen and sulfur compounds may also react within the atmosphere to form secondary inorganic aerosols (SIA) (Seinfeld & Pandis, 2016).

The Health Effects Institute (HEI) recently summarized the results of UFP source apportionment studies in both the U.S. and Europe from 1996 to 2011 (Health Effects Institute, 2013). HEI characterized motor vehicles as a leading source of UFP emissions, particularly near roadways. HEI also found stationary point sources to be important contributors to UFP emissions, particularly at further distances from roadways. HEI posited that the relative contributions of mobile and stationary UFP sources varies considerably within the U.S. depending on the geographic location, season, and time of day.

Amann et al. (2011) and Paasonen et al. (2016) modeled particle number direct emissions for North America and other regions of the world for 10 anthropogenic source sectors from 2010 to 2030 using the Greenhouse Gas–Air Pollution Interactions and Synergies (GAINS) model. The modeling results showed direct particle number emissions in North America of approximately 9×10^{26} particles annually. Road transportation accounted for just over one-half (4.8×10^{26}) and nonroad transportation accounted for approximately one-fourth (1.8×10^{26}) of 2010 annual direct particle number emissions (Figs. 3–2). Fleet turnover of on-road and non-road mobile sources to vehicles and equipment meeting more stringent PM standards in the U.S. and Canada is expected to significantly reduce particle number emissions from mobile sources in North America by 2030. However, they are expected to remain significant sources of anthropogenic particle number emissions.

The top 2 sources of ultrafine number shown by Paasonen et al. (2016) are road transport and non-road transport. On the other hand, the top 2 sources of ultrafine mass, PM0.1, shown by Venecek et al. (2019) are natural gas combustion and food cooking. Kuwayama et al. (2013) shows a strong correlation between PM0.1 and surface area, but a weaker one between ultrafine number and surface area. Thus, individual metrics of ultrafine particles may not be well correlated. This highlights the importance of using all three moments (number, surface area, mass) when analyzing source emissions to realize the importance of their contribution. While the number metric is applicable to UFP below 100 nm since most of the particle number is below such size, the choice of PM0.1, as can be seen from Figs. 2–3, could miss a substantial fraction of the mass above that size within a continuous size distribution. Thus, the choice of PM0.1 cannot be supported as it omits a sizable fraction of PM mass from mobile sources. In the Recommendations section below, we are proposing a definition with an upper size limit of 500 nm which is more inclusive of all three moments.

4. UFP measurements

4.1. On-road and near-road size distributions

4.1.1. Near roadway and near proximity sampling of mobile sources—The association between traffic and UFP has been known for many years. Figs. 4–1 a shows measured surface area and calculated number weighted size distributions upwind and downwind of a California freeway in the early 1970s (Whitby et al., 1975). Number concentrations were not reported by Whitby but have been calculated here from his surface area measurements Figs. 4–1 b shows the difference between the upwind and downwind number weighted and surface area weighted size distributions shown in Figs. 4–1a. Nearly the entire number and surface area added by the roadway vehicle traffic is in the currently accepted UFP range, i.e., below 100 nm in mobility diameter.

Figs. 4–2 (Nanzetta & Holmén, 2004) shows some more recent, but similar comparisons between particle size distributions measured upwind and downwind of a California freeway, I-80, between San Francisco and Sacramento. These distributions are number rather than surface area weighted and show that most of the number added by the roadway is very small in diameter, having mobility diameters below about 25 nm. Their work contains a detailed analysis of the influence of meteorology, traffic volume and vehicle engine type (diesel or gasoline) on roadside particle size distributions.

Figs. 4–3 a shows roadside (10 m) and downwind (700 m) number weighted size distributions made near a Minnesota urban freeway (Kittelson, Watts, & Johnson, 2004). The roadside measurement shows a large ultrafine mode, mainly below 25 nm that has largely disappeared downwind. Figs. 4–3b and c show total number concentrations and the corresponding size distributions during measurement traverses perpendicular to an interstate highway at distances ranging from 30 to 312 m from the highway (Jacobson et al., 2005). Nanoparticles smaller than 30 nm dominate particle number and decrease with distance while the concentration of larger particles, presumably background aerosol, is largely independent of distance from the roadway. The decay of nanoparticle concentration with distance is reasonably described by an exponential decay with a characteristic distance of 92 m. The decay is likely a result of a combination of dilution, evaporation, and coagulation (Jacobson et al., 2005).

Figs. 4–1, Figs. 4–2, and Figs. 4–3a and Figs. 4–3c all show distinct nucleation modes with most of the number below 25 nm. It is worth noting how much things improved from 1975 to 2005 with peak downwind values for $dN/dLogD_p$ of $4.5 \times 10,^6$ $2 \times 10,^5$ $2.5 \times 10,^5$ and 3.5×10^4 particles/cm^3 for Whitby (CA, 1975), Nanzetta (CA, 2004), Jacobson (MN, 2005), and Kittelson (MN, 2004a).[8]

Zhu et al. (2002a, 2002b) measured the decay of particle number, black carbon, and CO downwind of two major California freeways, the I-710 with 25% diesel engine and the I-405 with only 5% diesel engine vehicle traffic. They found all species decayed rapidly downwind of the roadway with characteristic decay distances ranging from 13 to 46 m, faster decay than observed by Jacobson et al. (2005). The faster decay observed by Zhu et al. (2002a, 2002b) may be associated with higher traffic density and number concentrations leading to more rapid mixing, evaporation, and coagulation.

Saha et al. (2018) measured particle number size upwind and downwind of highway I-40 in North Carolina, USA. Fig. 4-4 (a) through (d) show average downwind particle number size distributions without background corrections at different distances from the roadway edge with the wind consistently coming off the highway. Fig. 4-4 (e) and (f) illustrate the background-subtracted downwind average particle number size distributions at 10 m (red) and 150 m (purple) distances. Diluting the distribution measured at 0 m using the dilution factor at 150 m, determined from the decay profile of BC, results in the red curve. Dilution alone explains the reduced number shown with orange shading, but other processes are

[8]Strictly speaking, we should compare area under the curve of size distribution instead of peak height, but the general trend is clear.

required to explain the red shaded portion, likely a combination of loss of semi-volatile material and coagulation.

4.1.2. On-road measurements compared to near road—Vehicle PM emissions measurements made on-road in diesel truck traffic with a mobile emissions laboratory (Kittelson et al., 2001, 2002) exhibit a very similar size structure to downwind roadside measurements, but the concentrations are considerably higher. Figs. 4–5 a shows on-road size distributions measured with and without a thermal denuder which allowed solid and volatile particles to be differentiated (Kittelson, Watts, Johnson, et al., 2004). The results shown are the average of 60 h of on-road measurements made on a rural part of interstate I-90 in New York State. These measurements were made with a scanning mobility particle sizer (SMPS) and both number and volume (proportional to mass) weighted size distributions are shown. Note the clear modal structure with a nucleation mode in the 8 nm to about 50 nm range and an accumulation mode from about 50 nm to 300 nm. The upper and lower sizing limits of the SMPS used in this work were 8 and 300 nm and the bimodal lognormal fits shown on the plot indicate that the nucleation mode extends below 8 nm and the accumulation mode above 300 nm although most of the modes are captured. The use of the thermal denuder reveals the material in the nucleation mode is nearly all semi-volatile, 96% of the number is removed by the thermal denuder. On the other hand, about 65% of the volume in the accumulation mode is removed by the denuder. This is much more than one would expect if these were mainly carbonaceous soot particles. This is likely due to a significant amount of material in the accumulation mode that is background aerosol containing semi-volatile organic and inorganic compounds.

Figs. 4–5b shows particle size distributions from the same test series (Kittelson, Watts, Johnson, et al., 2004) grouped by ambient temperature. They have been normalized by dividing by total particle volume so that the relative size of the nucleation and accumulation modes may be seen. The relative size of the nucleation mode decreases with ambient temperature in the range from 9.6 to 23.2 °C. Figs. 4–6 shows a similar result but this time for on-road chase experiments that focused on emissions from a heavy-duty truck conducted as part of the CRC E–43 program (Kittelson et al., 2000, 2002). It shows size distributions measured in the plume of a heavy-duty truck measured under cruise and ambient conditions for ambient temperatures of 11 and 21 °C. There is little change in the accumulation mode with ambient temperature, but the nucleation mode is much smaller at the higher temperature.

Figs. 4–7 show the results of size distribution measurements made in the plume of a heavy-duty truck under on-road chase conditions, this time done with two different fuels: a pre-2006 U.S. low-sulfur diesel fuel with a sulfur content of approximately 350 ppm and a California low-sulfur diesel fuel with a sulfur content of less than 100 ppm.[9] The nucleation mode is much larger with the higher sulfur fuel suggesting the role of sulfuric acid in the formation of the nucleation mode (Shi & Harrison, 1999; Khalek et al., 2000; Maricq et al., 2002; Vaaraslahti et al., 2004). Arnold and coworkers (Arnold et al., 2006; Karjalainen

[9]Note that both the U.S. and California fuels pre-date the U.S. introduction of ultra-low-sulfur diesel fuel (ULSD) with S < 15 ppm in 2006.

et al., 2014; Pirjola et al., 2015) made direct measurements of sulfuric acid and organic vapors that demonstrated the role of sulfuric acid in nucleation and growth of engine exhaust nanoparticles. However, they also showed that there were conditions where sulfuric acid alone could not explain the nucleation process. They suggested that organic compounds also play a role and may participate in heteromolecular nucleation with sulfuric acid vapor.

4.2. UFP and PM mass measurement

4.2.1. Ambient sampling—Although there are monitoring stations reporting UFP to state and federal agencies, there are currently no U.S. EPA reference methods and there is no standardization for ambient or source UFP measurement. Measurement of UFP typically consists of sampling an aerosol followed by classification into one or more size ranges of interest followed by direct or indirect measurement of particle characteristics such as particle number, surface area, mass, or in some cases chemical composition (Baldauf, 2015). Sampling methods are available to determine each of these characteristics either by time-integrated sampling and subsequent sample analysis or by use of various on-line analyzers. Sampling, classification, and analysis of UFP is analogous to the approach taken for regulatory measurement of ambient fine PM mass, which uses direct ambient sampling through an inertial pre-classification stage with a D_p 50% cutpoint of 2.5 μm followed by sample integration via collection of fine PM on PTFE filter sample media (U.S. CFR, 2018a).

Classification of UFP size can be via the inertial, diffusional, or electrical mobility properties of the aerosol and sometimes more than one means of classification may be used. For example, the TSI 3031 UFP Monitor (TSI. (n.d.c)) uses a 1 μm cyclone (inertial) pre-classifier in addition to classifying particle size between 20 and 1000 nm into six submicron size bins by electrical mobility. In some cases, particularly in the case of condensation particle counters (CPCs), instrumentation has been used to measure UFP without size classification under the assumption that particles with D_p>100 nm do not significantly contribute to particle number measurements. However, UFP number may not necessarily be correlated with UFP mass because the relationship between particle number and mass depends on size, shape and density.

4.2.2. Direct sampling from mobile sources—UFP and PM mass sampling from internal combustion engine exhaust requires the use of well-defined, fundamental aerosol practices to minimize basic particle loss mechanisms related to diffusion, inertial impaction, interception, coagulation (which reduces number but conserves mass), settling, non-isokinetic sampling, electrostatic interactions, and thermophoresis (e.g., Friedlander, 2000; Fuchs, 1963; Hinds, 1999). However, in addition to these basic particle dynamic processes, there are other processes governing the sampling and measurement of volatile and semi-volatile materials that typically partition between the gas and particle phase during dilution and cooling of hot exhaust and subsequent aging in the sampling lines, instruments and on collection media. This process of gas to particle conversion during ambient dilution was illustrated in Figs. 2–1 and 2–2. The same processes occur during laboratory dilution, but it is impossible to exactly simulate the atmospheric process. Figs. 4–8 shows a typical laboratory dilution system that includes partial flow sampling and full flow constant volume

sampler (CVS). In a full flow CVS, the entire content of exhaust is diluted and the total flow rate in the tunnel is fixed as a constant volumetric flow. Thus, if engine exhaust flow increased the dilution ratio decreased. In a partial flow sampling system, a small portion of exhaust is extracted and diluted either at a fixed dilution ratio or with variable dilution ratios that are inversely proportional to engine exhaust flow rate, similar to full flow CVS.

Particle mass source measurements require one or more stages of dilution with air to achieve a stable aerosol composition and size and to prevent measurement saturation or overloading and, particularly in the case of mobile source measurements, water condensation. Examples include the CVS systems used for mobile source regulatory particulate matter measurements (U.S. CFR, 2018b), and partial-flow dilution (PFD) sampling systems which are used either for mobile source laboratory particulate matter measurements (U.S. CFR, 2018b) or as part of portable emissions measurement systems (PEMS) (U.S. CFR, 2018c). Significant care must be taken in the design of air-dilution sampling systems to prevent positive or negative sampling artifacts (Khalek, I. A., 2006b, p. 2).

For UFP measurements, heated or unheated dilutors are sometimes used for primary, secondary or tertiary sample dilution in some cases, and may be integrated into electrical mobility particle classifiers to prevent saturation of the electrometers and/or CPC during source measurements and measurement of high particle concentrations during ambient sampling. Excellent reviews of suitable instruments and measurement methods have been given by Burtscher (2005), Maricq and Maldonado (2010), and Giechaskiel et al. (2014).

4.2.2.1. Understanding sampling system parameter effects on mobile source PM.: There are many variables that influence volatile and semi-volatile aerosol formation and growth when sampling from engines, including:

- **Dilution :** Dilution ratio; Dilution air temperature; Dilution residence time or rate of dilution; Composition of dilution air (not including water); Water content in dilution air; Dilution air particle composition, concentration, and size
- **Exhaust gas sample :** Water content; Temperature and composition; Exhaust solid particle concentration
- **Transfer and sample line :** Temperature prior to dilution; Residence time prior to dilution; Residence time between dilution and measurement; Dilution system geometry and materials; Particle wall interactions, storage, and release

These variables will need to be operationally defined to achieve reproducible UFP laboratory measurements between different laboratories and within an individual laboratory. The selection of each variable boundary condition is not intended to mimic every possible atmospheric dilution process, but rather to devise a laboratory sampling system that can predict the potential to form particles during atmospheric dilution and cooling.

This section highlights examples of how such variables influence the measurement of UFP directly from vehicle and engine exhaust. Without operationally and tightly defining variables that impact particle nucleation and growth, it would be impossible to reproduce

"primary" particle number and size distribution measurements from engine or vehicle emissions measurements.

Khalek et al. (1998, 1999), Shi et al. (1999, 2000), Mathis et al. (2004), Lyyränen et al. (2004), and Samaras et al. (2005) all investigated aspects of the influence of dilution conditions on nanoparticle measurement under laboratory sampling conditions. Tables 4-1 summarizes the sensitivity of nucleation mode formation to dilution parameters and residence time.

Khalek et al. (1999) measured particle size distributions from the exhaust of a 1995 model year medium-duty diesel engine operating on low sulfur diesel fuel, 400 ppm S, using a variable residence time, two-stage dilution system in which exhaust was diluted to a modest level (primary dilution), aged to allow particle formation and growth, and then diluted again to effectively freeze/prevent further changes. They found conditions in the aging chamber such as primary dilution ratio [PDR=(mass of dilution air + mass of exhaust)/mass of exhaust], primary dilution temperature (PDT), residence time (RT), and to a lesser extent, relative humidity (RH) have a significant influence on nanoparticle formation, mainly in the nucleation mode (NM). The main role of secondary dilution was to freeze the aging process and reduce concentrations to a range suitable for the instruments. Secondary dilution did not significantly change the shape of the size distributions. Figs. 4–9a shows how changing the residence time in the aging chamber, RT, from 100 to 1000 ms increases the concentration in the NM by nearly two orders of magnitude. NM formation was also strongly influenced by PDR as shown in Figs. 4–9b. The concentration in the NM decreases by nearly two orders of magnitude, but there is little change in the concentration in the accumulation mode (AM) as dilution ratio is increased from 12 to 40. The size distribution becomes insensitive to the dilution process for PDRs above about 60, suggesting that the remaining particles are nonvolatile, likely ash in the NM and soot in the AM. They also did limited testing with an ultralow sulfur diesel fuel, ~10–20 ppm. This caused up to a 70% decrease in the concentration of the nucleation mode but little change in the accumulation mode.

Shi et al. (1999, 2000) conducted multiple detailed studies of the composition and size of particles produced by a medium-duty diesel engine of the same type as used by Khalek et al. (1999). Particle mass, bulk composition (elemental[10] and organic carbon,[11] nitrates and sulfates), and gaseous emission measurements were stable and repeatable, but size distributions, especially in the range below 50 nm showed great variation. Concentrations in this size range increased with RH. The influence of PDR on sub 50 nm concentrations depended on RH, usually the concentration increased with PDR at higher RH but decreased with PDR at lower RH.

Mathis et al. (2004) used a two-stage dilution system consisting of a porous wall dilutor, an aging chamber, and an ejector dilutor in series to study nanoparticle emissions from a light-duty diesel passenger car equipped with an oxidation catalyst. This dilution system was

[10]Elemental carbon is operationally defined. It is any carbonaceous material that survives a temperature of 860 °C on a quartz filter in an oxygen free environment and later oxidized in the presence of oxygen at a temperature greater than 500 °C.

[11]Organic carbon is operationally defined. It is any hydrocarbon or carbonaceous material that is collected on a quartz filter and desorbed in an oxygen free environment at a temperature up to 860 °C.

developed for the EU “Particulates” program and is described in detail by Samaras et al. (2005). The vehicle was tested on a chassis dynamometer at steady state condition of 50 kph using 320 ppm S fuel. They investigated the influence of PDR, and DT, RH, and RT in the aging chamber on nanoparticle formation. This dilution system and engine gave stable and repeatable size distributions. Their results were generally similar to those reported by Khalek et al. (1999), as may be seen in Tables 4-1 Increasing RT from 0.6 to 3.1 s increased the diameter of the NM but decreased its concentration. Figs. 4–10a shows the influence of PDT on NM concentrations, which decreased by over an order of magnitude as PDT increased from 17 to 40°C. The concentration and size of particles in the NM increased strongly as RH (Figs. 4–10b) was increased from 2 to 51%. They discussed the sensitivity of NM formation to dilution conditions in detail and proposed two dilution sensitivity indices to describe the sensitivity of NM formation to changes in PDT and PDR, one based on the ratio of NM number to AM number concentrations, the other based on the ratio of NM volume to AM volume. They used these indices to determine the combination of PDT and PDR giving the smallest sensitivity to dilution conditions. This led to the suggestion of two sampling windows, the first for stable measurement of NM number: PDR = 25, RT = 3 s, and PDT = 20 °C; the second for stable measurement of NM volume: PDR = 12, RT = 3 s and PDT = 32 °C. These recommendations were based on dry dilution, RH < 5%. The recommendations are based on a single engine and vehicle, but the general approach could be useful in developing a robust method for measuring semi-volatile NM particles.

Lyyränen et al. (2004) tested four dilution systems, (1.) a partial flow tunnel plus ejector, (2.) two stage ejector with heated first stage, (3.) heated porous wall plus ejector and (4.) a single stage porous wall dilutor. A medium-duty off-road diesel engine operating on 430 ppm S fuel served as the particle source. Tests were run at light load and heavy load at a single speed, but the heavy load condition showed little dilution dependence and only the light load results are discussed here. One of the objectives of their work was to demonstrate that heated dilution could allow stable and repeatable measurements of non-volatile particles. This was found to be the case for the heated porous tube and the heated ejector systems which gave similar results with little dilution dependence. In this case, most of the particles measured were found in the accumulation mode range around 50 nm but small nucleation modes in the 10–15 nm diameter range were also observed. On the other hand, the partial flow tunnel with cool, 25 °C, primary dilution air temperature plus ejector system showed a strong increase in NM concentration as the PDR was increased from 2.5 to 5.3. The single stage porous tube dilutor was tested with dilution ratios ranging from 10 to 167 with 25 °C dilution air. In this case the total number concentration trended generally downward with some variation and stabilized at dilution ratios above about 50. An unusual feature of these measurements is that there was no distinct nucleation mode and most of the variation was in the accumulation mode size range, ~ 50 nm, suggesting that this dilution system promoted growth of semi-volatile particles into this size range.

Nanoparticle formation during sampling is sensitive to other details of the dilution system design. Barnes (1999) identified the effect of sample transfer line temperature on nanoparticles, particularly at light load. He observed a significant reduction in nanoparticles with lower transfer line temperature for the same engine load. Wei et al. (2001) and Sasaki (2002) observed a decrease in NM with increasing sample line length even with heated

sample lines. In both these cases, the reductions were attributed to loss of semi-volatile material to the walls of the sample lines. Figs. 4–11a illustrates Wei's results.

Many researchers have observed significant sampling system storage and release effects and long stabilization times associated with semi-volatile particle measurement. Wei et al. (2001) showed the influence of desorption of stored semi-volatiles from a transfer tube on the size distribution, as shown in Figs. 4–11b. They showed a large increase in the number of nanoparticles followed by a slow decrease, approaching the original size distribution when the temperature of the transfer tube increased from 200 °C to 305 °C. Yokoi et al. (2001) observed an 80 percent increase in number emissions when operating at high load after the engine was left idling for about an hour beforehand. They also observed that after the transition from higher load to idling conditions, the number of particles increased by a factor of 6 as the engine exhaust cooled. Kittelson and Khalek (1999) also observed effects of engine and sampling system conditioning on nanoparticle emission measurements and highlighted the effects of particle storage and release. Figs. 4–12a and Figs. 4–12b show particle number concentrations and size distributions during a step change from stable idle to rated power. About 20 min of stabilization time was required at high engine load before a stable number concentration and size distribution were reached. Khalek et al. (1998) also observed long stabilization times for particle number measurements, especially during the second half of an ISO 11-mode test, when the engine was changed from a high speed, light load, low exhaust temperature condition (M5) to a high load, high exhaust temperature condition (M6). They suggested that this was due to release of semi-volatile materials stored in the engine and/or sampling system during lower temperature operation. Mamakos et al. (2004) and Samaras et al. (2005) reported on data collected as part of the EU "Particulates" program. Mamakos et al. reported unstable formation of nucleation modes, especially after transition from light load to heavy load. Samaras et al. described transient formation and decay of large nucleation modes, especially with higher sulfur fuels and catalyzed exhaust aftertreatment. They attributed this to formation, storage and release of sulfates.

4.2.2.2. On-road measurements compared with sampling system measurements.: Sasaki (2002) showed the influence of different dilution techniques in comparison to a chase experiment, shown in Figs. 4–13. They found a discrepancy in nanoparticle emissions between using the full flow CVS and the chase experiments for steady-state operation. The full flow CVS gave lower nanoparticle number concentrations than the chase experiments, but a prototype partial flow dilution system gave results close to those of the chase experiments. While this work showed the sensitivity of the nucleation mode to dilution conditions, it was done for a limited number of test conditions and may not be generalizable.

One of the goals of the CRC E–43 program (Kittelson et al., 2002) was to determine if a laboratory dilution system could be developed that would mimic nucleation mode formation under on-road conditions. The work includes comprehensive examinations of different dilution schemes with different engines, fuels and test locations including on-road, engine dynamometer, and chassis dynamometer. Some typical measured size distributions from that study are shown in Figs. 4–14. These tests were run with a heavy-duty diesel truck powered by a turbocharged, aftercooled diesel engine with electronic unit injectors

operating on low sulfur diesel fuel, 400 ppm. The engine was not equipped with an exhaust oxidation catalyst. Here three different dilution strategies are compared with on-road chase experiments using the same engine type, fuel, and load conditions matched as closely as possible. The three dilution systems were (1.) a CVS full flow dilution tunnel followed by an ejector dilutor, PDR ~ 3, PRH ~ 60%, (2.) a Sierra BG-1 porous wall dilutor followed by an ejector dilutor, PDR = 7.5, PRH <20%, and (3.) a two-stage, dual ejector dilutor system, PDR = 11, PRH <20%. All measured size distributions have been normalized by the total measured aerosol volume concentration from the size distributions [$(1/V_{total}) \times dN/dlog(D_p)$] to minimize the influence of uncertainties in on-road dilution ratios. This allows the shapes of the distributions to be seen more clearly. The modes in the on-road size distributions are somewhat narrower and more distinct than in lab measurements. The CVS plus ejector (CVS) and the BG-1 plus ejector systems (BG1) gave relatively good agreement with on-road measurements. On the other hand, measurements using the two-stage ejector diluter (2-stage) underestimated the nucleation mode size and concentration. This was unexpected because this system was very similar to that described by Khalek et al. (1999) which produced large nucleation modes with similar dilution conditions. The only significant difference between the systems was that the heated transfer line from the tailpipe to first stage dilution was much longer, 27 inches, compared to 6–9 inches used by Khalek et al. As described above, both Sasaki and Wei observed that longer residence time in the transfer line before primary dilution (or longer sample line length) led to adsorption of semi-volatile materials on the walls and suppression of nucleation mode formation.

Vogt et al. (2003) measured exhaust particle size distributions under laboratory and on-road chase conditions using two Euro 3 diesel passenger cars. They investigated the influence of sampling and dilution conditions, fuel sulfur content and the exhaust oxidation catalyst on the formation of a nucleation mode. Figs. 4–15 shows typical results from on-road chase experiments. They found that the combination of low sulfur fuel (360 ppm) and an oxidation catalyst led to the formation of a large nucleation mode which took 25 min to form and stabilize under steady on-road conditions at 100 kph, although exhaust and catalyst temperatures were stable after only 5 min. They suggested that this may have been due to storage of sulfuric acid in the catalyst that became saturated after 25 min. Either removing the oxidation catalyst or running ultra-low sulfur diesel (ULSD) fuel having ≤10 ppm sulfur[12] led to the elimination of the nucleation mode with little impact on the accumulation mode. They also tested the vehicle with the oxidation catalyst installed running on 40 ppm sulfur fuel on-road at 100 kph and under the same conditions on a chassis dynamometer using a rotating disk dilutor operating at a dilution ratio of 100. The on-road and lab tests agreed well for the accumulation mode, but the nucleation mode did not form in either case. They did not do laboratory tests with the 360 ppm S fuel.

Giechaskiel et al. (2005) measured particle size distributions produced by a Euro 3 diesel passenger vehicle under on-road chase and laboratory conditions. The vehicle was equipped with an oxidation catalyst and operated on 280 ppm S fuel. The mobile laboratory was the same as used by Vogt et al. (2003). Laboratory tests were done on a chassis dynamometer

[12]European regulations refer to ULSD fuel having ≤10 ppm sulfur. U.S. regulations refer to ULSD fuel having ≤15 ppm sulfur.

using a partial flow sampling system consisting of a porous wall dilutor followed by ejector dilutors system like that developed for the EU “Particulates” program (Samaras et al., 2005). It allowed temperature, dilution ratio, and humidity in the primary dilution stage to be varied. Laboratory and on-road chase experiments were performed at 50, 100, and 120 kph and additional laboratory tests were performed at 100 and 120 kph, variable load. Figs. 4–16 compares on-road (a) and lab (b) size distributions measured at the 3 speeds. The accumulation modes measured were relatively independent of load and well matched between lab and chase experiments. Nucleation modes were formed both on-road and in the lab at 100 kph and 120 kph but not at 50 kph. Although nucleation mode particles formed both on-road and in the lab, the particles were smaller in the on-road experiments. The nucleation mode developed quickly at 120 kph but took some time to form at 100 kph as shown by the insets in the plots. Vogt et al. (2003) observed similar behavior. It was attributed to initial storage of sulfates in the catalyst. The dilution conditions in the lab tests at 50 and 100 kph were PDR = 12.6, 13.5; PDT = 32 °C, RT = 2.5 s, and RH < 5%. These are in the same range as those suggested by Mathis et al. (2004) for stable volume in the nucleation mode: PDR = 12, PDT = 32 °C, RT = 3 s and RH < 5%. However, for 120 kph, PDR had to be set higher, to 36, to prevent saturation of the instruments. These conditions were very different from the on-road test conditions where the overall dilution ratios ranged from 1800 to 7100, RT from 0.4 to 1 s, ambient temperature from 3 to 6 °C, and humidity from 50 to 55%. They also performed a series constant speed, variable load lab tests at 100 and 120 kph, PDR = 13–15, secondary dilution ratio = 1300, PDT = 32 °C, RT = 0.5 s, and RH < 5%. Stable nucleation modes were formed for a range of loads and speeds with concentration and size increasing with load. When tests were done at the same load and speed as the on-road chase tests, at 100 kph both the concentration and size were larger than on-road, but at 120 kph concentration was similar and size was larger than on-road. The authors discussed the difficulty of matching on-road and lab conditions but suggest that the persistence of the formation of the nucleation mode under both lab and on-road conditions indicates that it is a real exhaust component, not an artifact.

Rönkkö et al. (2006) compared on-road and laboratory size distributions using a Euro III compliant bus equipped with a catalytic convertor and running on 50 ppm S fuel. On-road measurements were done with a mobile laboratory trailing the bus at chase distances of 5 and 10 m which corresponded to nominal atmospheric residence times of 0.45 and 0.9 s and dilution ratios in the ranges of 200–600 and 600 to 800, respectively. Distinct nucleation modes formed for most on-road conditions. The geometric mean diameter (GMD) of the nucleation mode varied from about 5 to 18 nm, somewhat smaller than reported in earlier studies, likely because a nano-SMPS with a sizing range of 3–60 nm was part of the instrument suite. There was little difference in size and concentration of the nucleation mode at the two distances/residence times, suggesting that nucleation and growth was already frozen at the 5 m chase distance and dilution ratios of 200 or more. On the other hand, formation of the nucleation mode depended strongly on ambient temperature and humidity; concentrations increased with lower temperature and higher humidity. They conducted laboratory tests using a porous wall plus ejector system like that developed for the EU “Particulates” program (Samaras et al., 2005) that allowed temperature, dilution ratio, and humidity in the primary dilution stage to be varied. The concentration and size of the

nucleation mode decreased with increasing PDR in the range from 12 to 36. Using a PDR of 12 closely matched the GMD of the on-road nucleation mode but the concentration in the mode was consistently lower. This is illustrated in Figs. 4–17 which compares on-road and laboratory nucleation mode concentrations for a variety of dilution and driving conditions. The conditions shown are all at 40 kph with torque increasing from 332 to 714 Nm and exhaust temperature increasing from 240 to 310 °C, for conditions 5 to 8, respectively.

Keskinen and Rönkkö (2010) provided a thorough review of studies comparing nanoparticle measurements in the laboratory and during on-road chase experiments, including Rönkkö et al. (2006) described above. They conclude that while several studies have shown that although it is possible to match the size of nucleation mode particles measured on-road and in the laboratory, laboratory measurements generally underestimate the concentration of nucleation mode particles as shown in Figs. 4–18. This contrasts with the work of Giechaskiel et al. (2005) that showed that laboratory measurements overestimate particle size in the nucleation mode and either match or overestimate its concentration, depending on test conditions.

On-road nucleation mode formation is not only influenced by temperature and pressure but also by background particle concentration. Kittelson et al. (2000) performed a comparison between wind tunnel, chase, and near road experiments. For the wind tunnel experiments (Gautam et al., 2003), the same truck used in the on-road chase experiments was operated on a dynamometer in the wind tunnel under the same speed and load conditions as the on-road chase tests. The wind tunnel air was recirculated during the day so in-tunnel engine testing built up a significant background (soot) particle concentration from the engine PM emissions. The wind tunnel size distributions in Figs. 4–19 show that when the truck was running, the concentration of particles below 100 nm increased by a factor of 2–3 but no distinct nucleation mode formed. On the other hand, on-road chase experiments, where the background aerosol concentration was much lower, gave a very different size distribution with a large concentration in the nucleation mode size range. They suggested that the high background concentration of soot particles in the wind tunnel scavenged semi-volatile materials and suppressed nucleation. A similar effect was observed (Sturm et al., 2003) in long road tunnels where nucleation mode particles are found near the tunnel inlet, but gradually disappear when moving into the tunnel and as the background particle concentration builds up. Laboratory tests have also demonstrated that the presence of solid particles during dilution and cooling of engine exhaust can be crucially important to sampling volatile and semi-volatile nanoparticles. Khalek (2006a) showed the formation of nanoparticles may be suppressed in the presence of solid particles, as shown in Figs. 4–20.

4.3. Laboratory sampling and dilution processes

As is clear from the discussion above, measuring particles, especially semi-volatile particles, from engines in the laboratory can be greatly impacted by the dilution and sampling process. One can take two measurements from an engine operating at the same condition and get drastically different results, particularly in number emissions, depending on the sampling and dilution process used. While the range of atmospheric dilution processes cannot be captured in engine laboratories, several researchers (Mamakos et al., 2004; Mathis

et al., 2004; Samaras et al., 2005; Giechaskiel et al., 2005; Maricq & Maldonado, 2010) have articulated different approaches to how the measurement ought to be done in the laboratory to incorporate critical elements of the atmospheric dilution process and avoid suppression of nucleation and growth. Parameters that can impact particle formation and growth during particle sampling and dilution in the laboratory must be tightly controlled to minimize variability and enhance reproducibility. As discussed earlier, these parameters include, for example, dilution air temperature and dew point, residence time, dilution ratio, and the geometry of the dilution system and exhaust transfer line. While such variables may be adjusted to maximize particle nucleation and growth for a particular combination of engine, fuel, and test conditions, further research is needed to define them in such a way that the potential for nucleation and growth may be determined for a variety of engine, fuel, and test conditions. For example, Figs. 4–21 (Khalek, 2006b, p. 2) shows the dependence of the driving force for nucleation and growth, the saturation pressure ratio (partial pressure/vapor pressure), for C16 and C25 normal alkanes, representing diesel fuel and lubricating oil, respectively, on dilution ratio and exhaust temperatures assuming adiabatic dilution. Here the optimum dilution ratio ranges from about 15 to 50. Figs. 4–22, shows a similar dependence of sulfuric acid nucleation on dilution ratio and temperature. It shows the calculated the ratio of actual sulfuric acid concentration to the critical concentration necessary to trigger binary sulfuric acid/water nucleation. Critical concentrations are calculated using model from Seinfeld and Pandis (2016). In this case the optimum dilution ratio ranges from about 15 to 40. Thus, depending on exhaust temperature and exhaust species, there is a dilution ratio that leads to the maximum driving force for nucleation and growth, i.e., saturation pressure ratio (hydrocarbons) or critical concentration ratio (sulfuric acid). In these relatively simple models, which assume no sinks are present and that organic compounds are condensing/evaporating according to ideal mixing assumptions, the location of the maxima depends only on the species of interest and exhaust and dilution air temperatures. In the case of sulfuric acid, the water content of the exhaust and dilution air are important as well. When scavenging surfaces are present, e.g., sampling lines, especially before primary dilution and also particles in exhaust and dilution air, they act as sinks for semi-volatile species and suppress nucleation and growth. Figs. 4–23 (Khalek, 2006) shows the reduction of volatile species as a function of residence time with and without a high efficiency diesel particulate filter (DPF) in the engine exhaust. Calculations for Figs. 4–23 assume no interaction with the internal walls of the sampling system that may lead to additional volatile/semi-volatile losses. The influence of the presence of particles during dilution is shown in another way in Figs. 4–24. It shows the critical concentration ratio for sulfuric acid/water nucleation as a function of dilution ratio - but now both soot concentration and the rate of dilution must be considered. This process can be described using a dimensionless parameter Rads, defined as the ratio of the rate of adsorption onto existing particles to the rate of dilution. As Rads increases, the optimum dilution ratio and maximum concentration ratio decrease. When Rads is high due to a high concentration of solid particles and/or slow dilution, then the concentration ratio is reduced, below 1, suppressing nucleation. On the other hand, when the Rads is low due to the lack of solid particles and/or fast dilution, the peak concentration ratio is high, for this example where the concentration ratio is above 1, likely triggering nucleation. However, although fast dilution makes nucleation more likely, it also leaves little time for particle growth. The

suppression of nucleation due to the presence of particle surface area during dilution was observed experimentally as described above in discussion of Figs. 4–19 and Figs. 4–20.

As can be seen from this discussion, choosing a single set of dilution parameters that can simulate nucleation and growth for every case of atmospheric dilution with highly variable temperature, humidity, and dilution rate is impossible. However, defining a set of dilution variables that favor nucleation and growth of semi-volatile particles and at the same time minimize the sensitivity to small changes in dilution and test conditions may be possible.

4.4. Issues associated with defining UFP

As discussed above, there is no consistent definition in the literature of what is meant by UFP. In addition, in some cases, there is no mention of the metric (number, surface area, or mass) associated with the UFP study nor the definition of particle diameter (aerodynamic, electrical mobility, etc.) related to UFP. Based on laboratory measurements of particle size distributions accumulated from mobile sources over the years, one could define UFP as particle number below 100 nm as over 95% of the particle number typically resides below 100 nm. However, as was shown in the size distribution in Figs. 2–3, there is an appreciable surface area and mass of particles larger than 100 nm in diameter. For surface area and mass, defining UFP to be below 100 nm would miss a significant fraction of those metrics. We suggest that a more appropriate definition of source, roadway and near roadway UFP from combustion sources are particles below 500 nm in diameter as discussed in detail in section 5.2. This definition captures all moments of the size distribution such as number, surface area, volume, and mass. Measurement of a continuous size distribution covering this size range would, for example, allow a researcher doing a health study on UFP number from mobile sources to isolate the impact of other moments, such as surface area and mass, because all metrics would be captured. Thus, it is crucial to not only define UFP but to also capture the metrics associated with it.

5. Recommendations

5.1. Laboratory sampling and dilution system

It is clear from the discussion above that semi-volatile materials are an important constituent of engine exhaust. Because one of the objectives in defining mobile source UFP measurements is to have an indicator of ambient UFP exposure and for the measurement to be reasonably representative of what is in the on-road and near road, we recommend sampling and measurement of both non-volatile and semi-volatile PM components rather than adopting a non-volatile method like that used for certification tests in the EU (Giechaskiel, 2012; Lähde & Giechaskiel, 2021; Samaras et al., 2020). For laboratory measurement of UFP emitted from engines and vehicles, we recommend the use of an operationally defined partial flow dilution system that include tight boundary conditions of various dilution parameters such as transfer line residence time, dilution and mixing geometry, dilution air temperature and relative humidity, and dilution ratio and residence time. Such a system will be intended to favor particle nucleation and growth using what we know about the impact of dilution parameters and other variables but provides less variability and more reproducible results. Uncertainty analyses will need to be performed

on such systems to determine the boundary conditions acceptable for each dilution variable. Partial flow sampling systems provide the flexibility to measure particle emissions from a variety of engine sources similarly regardless of engine size and horsepower rating. They provide the flexibility to measure particle emissions for both steady-state and transient engine operation. This approach was also supported by Ntziachristos and Samaras (2010) for using partial flow at a constant dilution ratio. While more research is needed on this topic to establish a robust and consistent particle measurement system for total particle number, surface area and mass, we know enough to establish basic guidelines for researchers. These are not suggestions for regulation. Based on the work described in this manuscript, we recommend the following parameters and boundary conditions:

a. **Partial flow sampling system for particle sampling:** This system provides flexibility to sample particles from different engine or vehicle platforms similarly, regardless of their size, power and operation. It will establish consistency for sampling particles from engines.

b. **Heated exhaust transfer line to 350°C with less than 100 ms residence time:** This is done to minimize loss of semi-volatile materials to the walls suppressing nucleation and potentially leading to subsequent storage and release as is shown in Figs. 4–11. This is important in reducing variability and artifacts in particle sampling.

c. **Dilution Ratio, Temperature and Residence Time:** A primary dilution ratio of 12, dilution air temperature of 25 °C and a residence time of 1.0–3.0 s seem to provide the right condition to enhance nucleation and growth, as supported by Khalek et al. (1999), Ntziachristos and Samaras (2010), and Kittelson and Khalek (1999). Although lower air temperature can provide more nucleation and growth as shown by Khalek et al. (2000), Mathis et al. (2004) and Kittelson et al. (2002), the 25 °C is recommended to represent a typical temperature used in engine laboratories for emissions certification. After the primary dilution condition is satisfied, a secondary dilution ratio can be used as needed to satisfy the measuring instrument requirement to avoid instrument saturation.

We do not recommend the use of heated dilution, either primary or secondary, because it suppresses the formation of semi-volatile particles, an important fraction of ambient aerosols.

d. **Relative Humidity (RH) in Dilution Air:** Khalek et al. (1999) showed enhancement of nucleation mode at higher RH, but other variables, namely residence time, primary dilution temperature and primary dilution ratio were found to be more significant variables. Mathis et al. (2004) made measurements with RH varying from 2% to 51% and showed a significant increase in nucleation mode concentration with increasing RH as depicted in Figs. 4–10b. However, these tests were done using a vehicle equipped with an oxidizing catalyst and operating on a relatively high sulfur content (323 ppm) fuel, much higher than ultra-low sulfur diesel fuel used today (<15 ppm in the U.S.). This combination would promote sulfuric acid aerosol formation which is very sensitive to relative humidity. Using dilution air with high relative humidity

would enhance nucleation mode formation but presents practical difficulties with water condensation especially for gasoline and natural gas vehicles that have a much higher water content in the exhaust than diesel. Furthermore, Mathis et al. (2004) and Giechaskiel et al. (2005) were able to produce significant and stable nucleation modes using dry dilution air (<5% RH). Therefore, we recommend that dry primary dilution air be used, RH <5%.

Many studies continue to use varied sampling and dilution procedures that often suppress the formation of semi-volatile particles. These inconsistencies make it difficult to compare studies and to understand the formation of these particles by modern engines. For example, Focsa et al. (2020), in a comprehensive study on the nature of particles emitted from a modern GDI engine used a two-stage dilution system with a heated first stage (180 °C). As we have seen from the discussion above, this will suppress the formation of semi-volatile particles. In another contemporary study, Di Iorio et al. (2021) examined particles from a PFI/GDI spark ignition engine fueled on gasoline and ethanol blends. Specific attention was paid to heated and unheated dilution to help understand the impact of semi-volatile particles. Unfortunately, however, the authors used a 1.5 m long sample line before primary dilution and a high primary dilution ratio of 79:1. Both would significantly suppress the formation of semi-volatile particles. These cited examples, although excellent and comprehensive, further highlight the difficulties of interpreting measurements of semi-volatile particles. These examples and many others discussed in this paper illustrate the need for a standardized dilution and sampling procedure.

5.2. New UFP definition and associated measurements

5.2.1. New UFP definition—Historically, UFP are defined as particles below 100 nm in diameter. However, this size range is misleading and only relevant to the number metric. Significant surface area and mass are present in the continuous size distribution in the size range between 100 nm and 500 nm, as shown in Figs. 5–1. Thus, the 500 nm definition is inclusive of all three moments and highlights the importance of capturing all three moments within epidemiological and laboratory studies. This will lead to a better understanding of potential causes and effects and to determine which moment of the size distribution may be more critical to human health effects relative to other size distribution moments. Although measuring the entire size distribution is the single most comprehensive approach to capture number, surface area and mass, converting a number size distribution into surface area or mass involves making assumptions about particle shape and density that require more research and understanding. Furthermore, a single sizing instrument may not capture the entire size range of interest from 3 nm to 500 nm and most current instruments are expensive. Until these issues are resolved and understood, single metric measurements with clearly defined size boundaries could be very useful. Such measurements would likely be much less expensive, allowing widespread deployment and critical evaluation of the impacts of each metric on human health. Moreover, coupling different single metrics, for example, number and LDSA, with assumptions, gives information on size and still may be relatively inexpensive. However, comprehensive size distribution measurements must continue; without them it would not have been possible to define the size range for single metric measurements. Size distribution measurements will continue to allow us to identify

refinements to UFP into the future. Furthermore, it is likely that a new generation of sizing instruments will be less expensive as discussed in 5.2.2.

Figs. 5–1 shows the particle number, surface area and mass distribution of mobile and other combustion sources as a function of both mobility (Dm) and aerodynamic diameter (Da). There is very little surface area or mass below 10 nm, thus the lower cut point will have little impact on surface or mass measurements. On the other hand, there is little number above 100 nm so the upper cut point will have little impact on number measurements. The sub 500 nm mobility diameter fraction captures slightly less of the mass and surface area, but it is likely that the differences would be small in practice. The difference between mobility and aerodynamic diameters is due to particle density, ρ_p; for $\rho_p > 1.0$ g/cm^3 Da > Dm while for $\rho_p < 1.0$ g/cm^3 Da < Dm. (Hinds, 1999). The density of freshly emitted engine particles decreases from greater than 1 g/cm^3 in the nucleation mode range to, for example, about 0.3–0.4 g/cm^3 at 300 nm in the accumulation mode (Maricq et al., 2000; Maricq & Xu, 2004; Park et al., 2003).

Our recommended sizing bounds are summarized in Tables 5-1. The choice between using a 500 nm aerodynamic or mobility diameter cut point may be dictated by practical considerations. For example, if a complete particle size distribution is available, in most cases the size distribution will be based on mobility diameter. On the other hand, if the sizing is done using an impactor system the cut point would be based on aerodynamic diameter. If a single metric is being measured, for example mass or surface area, using aerodynamic classification upstream of the measurement is an easy practical solution.

Unlike the upper cut point, a lower cut point is more difficult to define. It is clear from Figs. 5–1 that the lower sizing limit will have a strong influence on the total number count, but little impact on surface area or mass. Widely available and used instruments usually have a lower cut point in the range of 3–6 nm. These instruments include CPCs, scanning instruments and fast response size instruments. New measurement techniques developed have allowed measurements down to a diameter of 1 nm but these are not yet widely used for routine measurements (Iida et al., 2009; Vanhanen et al., 2011; Alanen et al., 2015; Rönkkö et al., 2017; Alanen et al., 2017).

Our recommendations as a practical matter going forward is a clearly stated lower cut point in the 3–6 nm diameter range. This recommendation takes into consideration CPCs with a lower cut point of 3 nm that have been available and widely used since the early 1990s, and available and widely used sizing instruments which have a lower cut point in the 3–6 nm range. If an instrument has a lower or higher cut point from the recommendation, it should be also clearly stated.

When a single metric measurement is being used for surface area, lung deposited surface area or mass, we recommend the use of an upstream inertial classifier with an aerodynamic diameter cut point of 500 nm. The choice of using an inertial separator to define UFP-M is comparable to current EPA definitions of PM_{10} and $PM_{2.5}$. In the case of number, we recommend the use of instruments with a lower size cut point of approximately 3 nm, clearly stated. Furthermore, no aerodynamic pre-classification is necessary as there is little

number present above 100 nm and even less above 500 nm. This definition, except for the specification of a lower size cut point, is nearly the same as the current commonly used definition of ultrafine particle number.

For some size distribution measurement instruments there is a pre-classifier at the inlet of the instrument as part of the instrument operation and data inversion. However, since size distribution data may be post processed to any desired upper cut point, no additional pre-classification of aerosol is required.

5.2.2. New UFP measurement approaches—One of the most comprehensive approaches to capturing all moments of the size distribution is to measure the number-weighted size distribution of particles using a conventional size measurement instrument either based on electrical mobility (e.g., TSI SMPS (TSI. (n.d.b)), TSI Engine Exhaust Particle Sizer [EEPS] (TSI. (n.d.b)), Cambustion Differential Mobility Spectrometer [DMS500] (.Cambustion. (n.d.)), GRIMM SMPS + C systems (GRIMM, n.d.)) or based on inertial classification (e.g., Dekati Electrical Low Pressure Impactor [ELPI+] (Dekati, n.d.)., TSI Microorifice Uniform Deposit Impactor [MOUDI] (TSI. (n.d.a))). The other moments of the size distribution such as surface area, volume and mass can be derived from the number weighted distribution. In the case of mass, the use of an effective density is needed to a volume distribution to a mass distribution (Maricq & Xu, 2004; McMurry et al., 2002; Park et al., 2003). The sizing instruments mentioned above are relatively expensive and complex. However, simpler and/or lower cost systems have been developed (Barmpounis et al., 2016; Kulkarni et al., 2016; Mei et al., 2011; Qi & Kulkarni, 2016; Todea et al., 2017) and initial systems have been commercialized, such as the Kanomax, n.d.-FMT PAMS (Kanomax, n.d.) or TSI NanoScan (TSI. (n.d.b)). Further development of low-cost number-based size distribution measurements for widespread use in engine emissions, atmospheric sampling, and health related research will be crucial at improving our understanding of the potential effects of UFP on human health.

In cases where it is or was not possible to measure a complete size distribution, the metric used must be defined. For example, a measurement of ultrafine number with a CPC should be called UFP-N, not UFP. Measurement of ultrafine surface area or more typically LSDA that is typically measured with a diffusion charger, (e.g., Naneos Partector (.Naneos. (n.d.)), Pegasor (Amanatidis et al., 2013), testo DiSCmini (.Testo. (n.d.))), should be called UFP-LDSA. An interesting aspect of LDSA is that it tends to capture both the nucleation and accumulation modes in a simple measurement, as shown in Figs. 5–1, and the instruments for measuring LDSA are relatively low cost and could be widely deployed. Measurement of UFP mass using for example 500 nm inertial classification in front of a filter, analogous to $PM_{2.5}$, should be called UFP-M. When simple instruments that measure a single metric, like a CPC and a diffusion charger are used together, then multiple metrics including particle size may be obtained if one assumes a unimodal log-normal size distribution.

Acknowledgements

Funding for this project was provided by the U.S. Environmental Protection Agency Office of Transportation and Air Quality (OTAQ) in Ann Arbor, MI. We like to acknowledge the support of Angela Cullen, Michael Olechiw, and Brian Nelson, the help of Patricia Klavon, Tricia Bosler, and Jennifer Mendenhall in submitting

this manuscript, Tom Veling who kindly reviewed the final draft of this manuscript, and Kinikachi Wejinya for helping with preparation of the figures. All of these individuals are from OTAQ. Mr. Wejinya was supported in part by an appointment to the Research Participation Program at the OTAQ, U.S. Environmental Protection Agency, administered by the Oak Ridge Institute for Science and Education through an interagency agreement between the U.S. Department of Energy and EPA. We also acknowledge Stephen McDow, Jason Sacks, and Ben Murphy from U.S EPA Office of Research and Development for their review and input into the manuscript.

References

Alanen J, Saukko E, Lehtoranta K, Murtonen T, Timonen H, Hillamo R, Karjalainen P, Kuuluvainen H, Harra J, Keskinen J, & Rönkkö T (2015). The formation and physical properties of the particle emissions from a natural gas engine. Fuel, 162, 155–161. 10.1016/j.fuel.2015.09.003

Alanen J, Simonen P, Saarikoski S, Timonen H, Kangasniemi O, Saukko E, Hillamo R, Lehtoranta K, Murtonen T, Vesala H, Keskinen J, & Rönkkö T (2017). Comparison of primary and secondary particle formation from natural gas engine exhaust and of their volatility characteristics. Atmospheric Chemistry and Physics, 17(14), 8739–8755. 10.5194/acp-17-8739-2017

Amanatidis S, Ntziachristos L, Samaras Z, Janka K, & Tikkanen J (2013). Applicability of the pegasor particle sensor to measure particle number, mass and PM emissions (SAE technical paper No. 2013-24–0167). SAE International. 10.4271/2013-24-0167

Amann M, Bertok I, Borken-Kleefeld J, Cofala J, Heyes C, Höglund-Isaksson L, Klimont Z, Nguyen B, Posch M, Rafaj P, Sandler R, Schöpp W, Wagner F, & Winiwarter W (2011). Cost-effective control of air quality and greenhouse gases in Europe: Modeling and policy applications. Environmental Modelling & Software, 26(12), 1489–1501. 10.1016/j.envsoft.2011.07.012

Arnold F, Pirjola L, Aufmhoff H, Schuck T, Lähde T, & Hämeri K (2006). First gaseous sulfuric acid measurements in automobile exhaust: Implications for volatile nanoparticle formation. Atmospheric Environment, 40(37), 7097–7105. 10.1016/j.atmosenv.2006.06.038

Baldauf RW, Devlin RB, Gehr P, Giannelli R, Hassett-Sipple B, Jung H, Martini G, McDonald J, Sacks JD, & Walker K (2016). Ultrafine particle metrics and research considerations: Review of the 2015 UFP workshop. International Journal of Environmental Research and Public Health, 13(11). 10.3390/ijerph13111054

Ban-Weiss GA, Lunden MM, Kirchstetter TW, & Harley RA (2010). Size-resolved particle number and volume emission factors for on-road gasoline and diesel motor vehicles. Journal of Aerosol Science, 41(1), 5–12. 10.1016/j.jaerosci.2009.08.001

Barmpounis K, Maisser A, Schmidt-Ott A, & Biskos G (2016). Lightweight differential mobility analyzers: Toward new and inexpensive manufacturing methods. Aerosol Science and Technology, 50(1), 2–5.

Barnes C (1999). August 9-10) the Sensitivity and Repeatability of nanoparticle Measurements at high dilution ratios [conference presentation]. In Proceedings of the 3rd international ETH workshop on nanoparticle measurement. Zurich, Switzerland http://www.nanoparticles.ch/archive/1999_Barnes_PR.pdf.

Beji A, Deboudt K, Khardi S, Muresan B, Flament P, Fourmentin M, & Lumière L (2020). Non-exhaust particle emissions under various driving conditions: Implications for sustainable mobility. Transportation Research Part D: Transport and Environment, 81, 102290. 10.1016/j.trd.2020.102290

Birch ME (2002). Occupational monitoring of particulate diesel exhaust by NIOSH method 5040. Applied Occupational and Environmental Hygiene, 17(6), 400–405. 10.1080/10473220290035390 [PubMed: 12049428]

Birch ME, & Cary RA (1996). Elemental carbon-based method for monitoring occupational exposures to particulate diesel exhaust. Aerosol Science and Technology, 25(3), 221–241. 10.1080/02786829608965393

Blanchard JD, & Willeke K (1983). An inhalation system for characterizing total lung deposition of ultrafine particles. American Industrial Hygiene Association Journal, 44(11), 846–856. 10.1080/15298668391405832

Brugge D, Patton AP, Bob A, Reisner E, Lowe L, Bright OJM, Durant JL, Newman J, & Zamore W (2015). Developing community-level policy and practice to reduce traffic-related air pollution exposure. Environmental Justice, 8(3), 95–104. [PubMed: 27413416]

Burtscher H (2005). Physical characterization of particulate emissions from diesel engines: A review. Journal of Aerosol Science, 36(7), 896–932. 10.1016/j.jaerosci.2004.12.001

Cambustion. (n.d.). DMS500 fast particle analyzer. Retrieved March 2, 2021 https://www.cambustion.com/products/branch/dms500-fast-particle-analyzer.

Cantrell BK, & Whitby KT (1978). Aerosol size distributions and aerosol volume formation for a coal-fired power plant plume. Atmospheric Environment, 12(1), 323–333. 10.1016/0004-6981(78)90214-7, 1967.

Cass GR, Hughes LA, Bhave P, Kleeman MJ, Allen JO, & Salmon LG (2000). The chemical composition of atmospheric ultrafine particles. Philosophical Transactions of the Royal Society of London,Series A: Mathematical, Physical and Engineering Sciences, 358(1775), 2581–2592. 10.1098/rsta.2000.0670

Chow JC, Watson JG, Chen LW, Arnott WP, Moosemuller H, & Fung KK (2004). Equivalence of elemental carbon by thermal/optical reflectance and transmittance with different temperature protocols. Environmental Science & Technology, 38(16), 4414–4422. [PubMed: 15382872]

Chow JC, Watson JG, Crow D, Lowenthal DH, & Merrifield T (2001). Comparison of IMPROVE and NIOSH carbon measurements. Aerosol Science and Technology, 34(1), 23–34. 10.1080/02786820119073

Clark WE, & Whitby KT (1967). Concentration and size distribution measurements of atmospheric aerosols and a test of the theory of self-preserving size distributions. Journal of the Atmospheric Sciences, 24(6), 677–687. 10.1175/1520-0469(1967)024<0677:CASDMO>2.0.CO;2

Daher N, Hasheminassab S, Shafer MM, Schauer JJ, & Sioutas C (2012). Seasonal and spatial variability in chemical composition and mass closure of ambient ultrafine particles in the megacity of Los Angeles. Environmental Sciences: Processes & Impacts, 15(1), 283–295. 10.1039/C2EM30615H

Dekati (n.d.). Real time particle measurement. Retrieved March 2, 2021 https://www.dekati.com/real-time-particle-measurement/.

Di Iorio S, Catapano F, Magno A, Sementa P, & Vaglieco BM (2021). Investigation on sub-23 nm particles and their volatile organic fraction (VOF) in PFI/DI spark ignition engine fueled with gasoline, ethanol and a 30% v/v ethanol blend. Journal of Aerosol Science, 153, 105723. 10.1016/j.jaerosci.2020.105723

Dick CAJ, Brown DM, Donaldson K, & Stone V (2003). The role of free radicals in the toxic and inflammatory effects of four different ultrafine particle types. Inhalation Toxicology, 15(1), 39–52. 10.1080/08958370304454 [PubMed: 12476359]

Donaldson K, & Stone V (2003). Current hypotheses on the mechanisms of toxicity of ultrafine particles. Annali Dell'Istituto Superiore Di Sanita, 39(3), 405–410.

Donaldson K, Stone V, Clouter A, Renwick L, & MacNee W (2001). Ultrafine particles. Occupational and Environmental Medicine, 58(3), 211–216. 10.1136/oem.58.3.211 [PubMed: 11171936]

Farwick zum Hagen FH, Mathissen M, Grabiec T, Hennicke T, Rettig M, Grochowicz J, Vogt R, & Benter T (2019). On-road vehicle measurements of brake wear particle emissions. Atmospheric Environment, 217, 116943. 10.1016/j.atmosenv.2019.116943

Ferin J, Oberdörster G, Penney DP, Soderholm SC, Gelein R, & Piper HC (1990). Increased pulmonary toxicity of ultrafine particles? I. Particle clearance, translocation, morphology. Journal of Aerosol Science, 21(3), 381–384. 10.1016/0021-8502(90)90064-5

Fierz M, Houle C, Steigmeier P, & Burtscher H (2011). Design, calibration, and field performance of a miniature diffusion size classifier. Aerosol Science and Technology, 45(1), 1–10. 10.1080/02786826.2010.516283.

Fissan H, Neumann S, Trampe A, Pui DYH, & Shin WG (2007). Rationale and principle of an instrument measuring lung deposited nanoparticle surface area. Journal of Nanoparticle Research, 9(1), 53–59. 10.1007/s11051-006-9156-8

Focsa C, Duca D, Noble JA, Vojkovic M, Carpentier Y, Pirim C, Betrancourt C, Desgroux P, Tritscher T, Spielvogel J, & Rahman M (2020). Multitechnique physico-chemical characterization

of particles generated by a gasoline engine: Towards measuring tailpipe emissions below 23 nm. Atmospheric Environment, 235, 117642. 10.1016/j.atmosenv.2020.117642

Friedlander SK (2000). Smoke, dust, and haze (2nd ed.). New York: Oxford University Press.

Fuchs NA (1963). On the stationary charge distribution on aerosol particles in a bipolar ionic atmosphere. Geofisica Pura e Applicata, 56(1), 185–193. 10.1007/BF01993343

Gautam M, Clark N, Mehta S, Boyce J, Rogers F, & Gertler A (2003). Concentrations and size distributions of particulate matter emissions from a class-8 heavy-duty diesel truck tested in a wind tunnel. SAE technical paper No. 2003-01-1894. SAE International. 10.4271/2003-01-1894

Gentner DR, Jathar SH, Gordon TD, Bahreini R, Day DA, El Haddad I, Hayes PL, Pieber SM, Platt SM, de Gouw J, Goldstein AH, Harley RA, Jimenez JL, Prévôt ASH, & Robinson AL (2017). Review of urban secondary organic aerosol formation from gasoline and diesel motor vehicle emissions. Environmental Science & Technology, 51(3), 1074–1093. 10.1021/acs.est.6b04509 [PubMed: 28000440]

Giechaskiel B, Mamakos A, Andersson J, Dilara P, Martini G, Schindler W, & Bergmann A (2012). Measurement of automotive nonvolatile particle number emissions within the European legislative framework: A review. Aerosol Science and Technology, 46(7), 719–749.

Giechaskiel B, Maricq M, Ntziachristos L, Dardiotis C, Wang X, Axmann H, Bergmann A, & Schindler W (2014). Review of motor vehicle particulate emissions sampling and measurement: From smoke and filter mass to particle number. Journal of Aerosol Science, 67, 48–86. 10.1016/j.jaerosci.2013.09.003

Giechaskiel B, Ntziachristos L, Samaras Z, Scheer V, Casati R, & Vogt R (2005). Formation potential of vehicle exhaust nucleation mode particles on-road and in the laboratory. Atmospheric Environment, 39(18), 3191–3198.

GRIMM (n.d.). SMPS-C. Retrieved July 29, 2021 https://www.grimm-aerosol.com/products-en/nanoparticle-sizers/smps-c/.

Harris SJ, & Maricq MM (2001). Signature size distributions for diesel and gasoline engine exhaust particulate matter. Journal of Aerosol Science, 32(6), 749–764. 10.1016/S0021-8502(00)00111-7

Harrison RM, Shi JP, Xi S, Khan A, Mark D, Kinnersley R, & Yin J (2000). Measurement of number, mass and size distribution of particles in the atmosphere. Philosophical Transactions of the Royal Society of London,Series A: Mathematical, Physical and Engineering Sciences, 358(1775), 2567–2580. 10.1098/rsta.2000.0669

Health Effects Institute. (2013). Understanding the health effects of ambient ultrafine particles. Boston, MA: HEI Perspectives 3 Health Effects Institute. https://www.healtheffects.org/publication/understanding-health-effects-ambient-ultrafine-particles.

Hinds WC (1999). Aerosol technology: Properties, behavior, and measurement of airborne particles. Wiley.

van de Hulst HC (1981). Light scattering by small particles. Dover Publications (Original work published 1957).

Husar RB, & Whitby KT (1973). Growth mechanisms and size spectra of photochemical aerosols. Environmental Science & Technology, 7(3), 241–247. [PubMed: 22236300]

Iida K, Stolzenburg MR, & McMurry PH (2009). Effect of working fluid on sub-2 nm particle detection with a laminar flow ultrafine condensation particle counter. Aerosol Science and Technology, 43(1), 81–96. 10.1080/02786820802488194

Iijima S (1984). Ultra-fine spherical particles of δ-alumina: Electron microscopy of crystal structure and surface morphology at atomic resolution. Japanese Journal of Applied Physics, 23(6A), L347. 10.1143/JJAP.23.L347

Iijima S (1985). Electron microscopy of small particles. Journal of Electron Microscopy, 34(4), 249–265. 10.1093/oxfordjournals.jmicro.a050518

International Commission on Radiological Protection. (1994). Human respiratory tract model for radiological protection. A report of a task group of the international commission on radiological protection. Annals of the ICRP, 24(1–3), 1–482. https://www.icrp.org/publication.asp?id=ICRP%20Publication%2066.

Jacobson MZ, Kittelson DB, & Watts WF (2005). Enhanced coagulation due to evaporation and its effect on nanoparticle evolution. Environmental Science & Technology, 39(24), 9486–9492. 10.1021/es0500299 [PubMed: 16475326]

Johnson BT, Hargrave GK, Reid B, & Page VJ (2011). Crankcase sampling of PM from a fired and motored compression ignition engine. SAE International Journal of Engines, 4(2), 2498–2509. 10.4271/2011-24-0209

Johnson JP, Kittelson DB, & Watts WF (2005). Source apportionment of diesel and spark ignition exhaust aerosol using on-road data from the Minneapolis metropolitan area. Atmospheric Environment, 39(11), 2111–2121. 10.1016/j.atmosenv.2004.12.018

Kanomax. (n.d.). Pams (portable Aerosol mobility spectrometer) - Kanomax FMT. Retrieved March 2, 2021 https://www.kanomaxfmt.com/product/pams-portable-aerosol-mobility-spectrometer/.

Karjalainen P, Rönkkö T, Pirjola L, Heikkilä J, Happonen M, Arnold F, Rothe D, Bielaczyc P, & Keskinen J (2014). Sulfur driven nucleation mode formation in diesel exhaust under transient driving conditions. Environmental Science & Technology, 48(4), 2336–2343. 10.1021/es405009g [PubMed: 24471707]

Keskinen J, & Rönkkö T (2010). Can real-world diesel exhaust particle size distribution be reproduced in the laboratory? A critical review jorma keskinen. Journal of the Air & Waste Management Association, 60(10), 1245–1255. 10.3155/1047-32f89.60.10.1245

Khalek IA (2006, May 1). Volatile nanoparticle number emissions from a diesel engine equipped with a catalyzed particle filter. Los Angeles, CA, USA: Ultrafine Particle Conference.

Khalek IA (2006b). 2007 Diesel particulate measurement research (p. 2). CRC Project E-66 Phase. http://crcsite.wpengine.com/wp-content/uploads/2019/05/E-66-Phase-2-Final-Report-IAK-R5.pdf.

Khalek IA (2006c). Characterization of particle size, number, and mass emissions from a diesel powered generator. In ASME 2006 internal combustion engine division fall technical conference (ICEF2006) (pp. 9–15). 10.1115/ICEF2006-1533

Khalek I, Badshah H, Premnath V, & Brezny R (2018). Solid particle number and ash emissions from heavy-duty natural gas and diesel w/SCRF engines, SAE technical paper 2018-01-0362. SAE International. 10.4271/2018-01-0362

Khalek IA, Blanks MG, & Merritt PM (2013). Phase 2 of the advanced collaborative emissions study (Vol. 2). CRC Report. ACES Phase http://crcsite.wpengine.com/wp-content/uploads/2019/05/03-17124_CRC-ACES-Phase2-FINAL-Report_Khalek-R6-SwRI.pdf.

Khalek IA, Blanks MG, Merritt PM, & Zielinska B (2015). Regulated and unregulated emissions from modern 2010 emissions-compliant heavy-duty on-highway diesel engines. Journal of the Air & Waste Management Association, 65(8), 987–1001. 10.1080/10962247.2015.1051606 [PubMed: 26037832]

Khalek IA, Bougher TL, Merritt PM, & Zielinska B (2011). Regulated and unregulated emissions from highway heavy-duty diesel engines complying with U.S. Environmental protection agency 2007 emissions standards. Journal of the Air & Waste Management Association, 61(4), 427–442. 10.3155/1047-3289.61.4.427 [PubMed: 21516938]

Khalek IA, Kittelson DB, & Brear F (1999). The influence of dilution conditions on diesel exhaust particle size distribution measurements. SAE technical paper No. 1999-01–1142. SAE International. 10.4271/1999-01-1142

Khalek IA, Kittelson DB, & Brear F (2000). Nanoparticle growth during dilution and cooling of diesel exhaust: Experimental investigation and theoretical assessment. SAE technical paper No. 2000-01–0515. SAE International. 10.4271/2000-01-0515

Khalek ISA, Kittelson DB, Graskow BR, Wei Q, & Bear F (1998). Diesel exhaust particle size: Measurement issues and trends. SAE technical paper No. 980525. SAE International. 10.4271/980525

Kittelson DB (1998). Engines and nanoparticles: A review. Journal of Aerosol Science, 29(5), 575–588. 10.1016/S0021-8502(97)10037-4

Kittelson DB, Johnson J, Watts W, Wei Q, Drayton M, Paulsen D, & Bukowiecki N (2000). Diesel aerosol sampling in the atmosphere, SAE technical paper No. 2000-01–2212. SAE International. 10.4271/2000-01-2212

Kittelson DB, & Khalek IA (1999). January 18-20). Formation of nanoparticles during exhaust dilution. In EFI members conference: Fuels, lubricants engines, & emissions.

Kittelson DB, & Kraft M (2015). particle formation and models. In Crolla D, Foster DE, Kobayashi T, & Vaughan N (Eds.), Encyclopedia of automotive engineering: Part 1: Engines-fundamentals (1st ed., pp. 107–130). Wiley.

Kittelson DB, Watts W, & Johnson J (2001). March 26-28). Particle Measurement Methodology: On-road and laboratory measurements of nanoparticles from Diesel engines. San Diego, CA: Proceedings of the 11th CRC On-Road Vehicle Emissions Workshop.

Kittelson DB, Watts W, & Johnson J (2002). Diesel aerosol sampling methodology–CRC E-43. Final report. Coordinating Research Council. http://crcsite.wpengine.com/wp-content/uploads/2019/05/E-43-Final-Report.pdf.

Kittelson DB, Watts WF, & Johnson JP (2004). Nanoparticle emissions on Minnesota highways. Atmospheric Environment, 38(1), 9–19. 10.1016/j.atmosenv.2003.09.037

Kittelson DB, Watts WF, & Johnson JP (2006). On-road and laboratory evaluation of combustion aerosols—Part 1: Summary of diesel engine results. Journal of Aerosol Science, 37(8), 913–930. 10.1016/j.jaerosci.2005.08.005

Kittelson DB, Watts WF, Johnson JP, Remerowki ML, Ische EE, Oberdörster G, Gelein RM, Elder A, Hopke PK, Kim E, Zhao W, Zhou L, & Jeong C-H (2004). On-road exposure to highway aerosols. 1. Aerosol and gas measurements. Inhalation Toxicology, 16(sup1), 31–39. 10.1080/08958370490443024 [PubMed: 15204791]

Kittelson DB, Watts WF, Johnson JP, Schauer JJ, & Lawson DR (2006). On-road and laboratory evaluation of combustion aerosols—Part 2: Summary of spark ignition engine results. Journal of Aerosol Science, 37(8), 931–949. 10.1016/j.jaerosci.2005.08.008

Kulkarni P, Qi C, & Fukushima N (2016). Development of portable aerosol mobility spectrometer for personal and mobile aerosol measurement. Aerosol Science and Technology, 50(11), 1167–1179.

Kuwayama T, Ruehl CR, & Kleeman MJ (2013). Daily trends and source apportionment of ultrafine particulate mass (PM0.1) over an annual cycle in a typical California city. Environmental Science & Technology, 47(24), 13957–13966. 10.1021/es403235c [PubMed: 24245739]

Lähde T, & Giechaskiel B (2021). Particle number emissions of gasoline, compressed natural gas (CNG) and liquefied petroleum gas (LPG) fueled vehicles at different ambient temperatures. Atmosphere, 12(7), 893. 10.3390/atmos12070893

Lanzinger S, Schneider A, Breitner S, Stafoggia M, Erzen I, Dostal M, Pastorkova A, Bastian S, Cyrys J, & Zscheppang A (2016). Associations between ultrafine and fine particles and mortality in five central European cities—results from the UFIREG study. Environment International, 88, 44–52. [PubMed: 26708280]

Lyyränen J, Jokiniemi J, Kauppinen EI, Backman U, & Vesala H (2004). Comparison of different dilution methods for measuring diesel particle emissions. Aerosol Science and Technology, 38(1), 12–23. 10.1080/02786820490247579

Mamakos A, Ntziachristos L, & Samaras Z (2004). Comparability of particle emission measurements between vehicle testing laboratories: A long way to go. Measurement Science and Technology, 15(9), 1855–1866. 10.1088/0957-0233/15/9/024

Maricq MM, Chase RE, Xu N, & Laing PM (2002). The effects of the catalytic converter and fuel sulfur level on motor vehicle particulate matter emissions: Light duty diesel vehicles. Environmental Science & Technology, 36(2), 283–289. [PubMed: 11827064]

Maricq MM, & Maldonado H (2010). Directions for combustion engine aerosol measurement in the 21st century. Journal of the Air & Waste Management Association, 60(10), 1165–1176. [PubMed: 21090546]

Maricq MM, Podsiadlik DH, & Chase RE (2000). Size distributions of motor vehicle exhaust PM: A comparison between ELPI and SMPS measurements. Aerosol Science & Technology, 33(3), 239–260.

Maricq MM, & Xu N (2004). The effective density and fractal dimension of soot particles from premixed flames and motor vehicle exhaust. Journal of Aerosol Science, 35(10), 1251–1274.

Mathis U, Ristimäki J, Mohr M, Keskinen J, Ntziachristos L, Samaras Z, & Mikkanen P (2004). Sampling conditions for the measurement of nucleation mode particles in the exhaust of a diesel vehicle. Aerosol Science and Technology, 38(12), 1149–1160. 10.1080/027868290891497

Maynard AD, & Kuempel ED (2005). Airborne nanostructured particles and occupational health. Journal of Nanoparticle Research, 7(6), 587–614. 10.1007/s11051-005-6770-9

McDonald J (2021). Particulate matter emissions from light-duty vehicles equipped with port fuel injection and gasoline direct injection. Memo to Docket No. EPA-HQ-OAR-2021-0208. June 8, 2021.

McMurry PH, Wang X, Park K, & Ehara K (2002). The relationship between mass and mobility for atmospheric particles: A new technique for measuring particle density. Aerosol Science and Technology, 36(2), 227–238. 10.1080/027868202753504083

Mei F, Fu H, & Chen DR (2011). A cost-effective differential mobility analyzer (cDMA) for multiple DMA column applications. Journal of Aerosol Science, 42(7), 462–473.

Melton LA (1984). Soot diagnostics based on laser heating. Applied Optics, 23(13), 2201–2208. 10.1364/AO.23.002201 [PubMed: 18212972]

Morawska L, Ristovski Z, Jayaratne ER, Keogh DU, & Ling X (2008). Ambient nano and ultrafine particles from motor vehicle emissions: Characteristics, ambient processing and implications on human exposure. Atmospheric Environment, 42(35), 8113–8138. 10.1016/j.atmosenv.2008.07.050

Naneos. (n.d.). PARTECTOR the world's smallest nanoparticle detector. Retrieved March 2, 2021 https://www.naneos.ch/partector.html.

Nanzetta MK, & Holmén BA (2004). Roadside particle number distributions and relationships between number concentrations, meteorology, and traffic along a northern California freeway. Journal of the Air & Waste Management Association, 54(5), 540–554. 10.1080/10473289.2004.10470926 [PubMed: 15149042]

Ntziachristos L, & Samaras Z (2010). The potential of a partial-flow constant dilution ratio sampling system as a candidate for vehicle exhaust aerosol measurements. Journal of the Air & Waste Management Association, 60(10), 1223–1236. 10.3155/1047-3289.60.10.1223

Oberdörster G, Celein RM, Ferin J, & Weiss B (1995). Association of particulate air pollution and acute mortality: Involvement of ultrafine particles? Inhalation Toxicology, 7(1), 111–124. 10.3109/08958379509014275 [PubMed: 11541043]

Oberdörster G, Ferin J, Finkelstein G, Wade P, & Corson N (1990a). Increased pulmonary toxicity of ultrafine particles? II. Lung lavage studies. Journal of Aerosol Science, 21(3), 384–387. 10.1016/0021-8502(90)90065-6

Oberdörster G, Stone V, & Donaldson K (2007). Toxicology of nanoparticles: A historical perspective. Nanotoxicology, 1(1), 2–25. 10.1080/17435390701314761

Oberdörster G, & Yu CP (1990b). The carcinogenic potential of inhaled diesel exhaust: A particle effect? Journal of Aerosol Science, 21, S397–S401. 10.1016/0021-8502(90)90265-Y

Paasonen P, Kupiainen K, Klimont Z, Visschedijk A, Denier van der Gon HAC, & Amann M (2016). Continental anthropogenic primary particle number emissions. Atmospheric Chemistry and Physics, 16(11), 6823–6840. 10.5194/acp-16-6823-2016

Park K, Cao F, Kittelson DB, & McMurry PH (2003). Relationship between particle mass and mobility for diesel exhaust particles. Environmental Science & Technology, 37(3), 577–583. 10.1021/es025960v [PubMed: 12630475]

Pirjola L, Karl M, Rönkkö T, & Arnold F (2015). Model studies of volatile diesel exhaust particle formation: Are organic vapours involved in nucleation and growth? Atmospheric Chemistry and Physics, 15(18), 10435–10452. 10.5194/acp-15-10435-2015

Qi C, & Kulkarni P (2016). Miniature differential mobility analyzer for compact field-portable spectrometers. Aerosol Science and Technology, 50(11), 1145–1154.

Rönkkö T, Kuuluvainen H, Karjalainen P, Keskinen J, Hillamo R, Niemi JV, Pirjola L, Timonen HJ, Saarikoski S, Saukko E, Järvinen A, Silvennoinen H, Rostedt A, Olin M, Yli-Ojanperä J, Nousiainen P, Kousa A, & Maso MD (2017). Traffic is a major source of atmospheric nanocluster aerosol. Proceedings of the National Academy of Sciences, 114(29), 7549–7554. 10.1073/pnas.1700830114

Rönkkö T, & Timonen H (2019). Overview of sources and characteristics of nanoparticles in urban traffic-influenced areas. Journal of Alzheimer's Disease, 72(1), 15–28. 10.3233/JAD-190170

Rönkkö T, Virtanen A, Vaaraslahti K, Keskinen J, Pirjola L, & Lappi M (2006). Effect of dilution conditions and driving parameters on nucleation mode particles in diesel exhaust: Laboratory and on-road study. Atmospheric Environment, 40(16), 2893–2901. 10.1016/j.atmosenv.2006.01.002

Roth P, & Filippov AV (1996). In situ ultrafine particle sizing by a combination of pulsed laser heatup and particle thermal emission. Journal of Aerosol Science, 27 (1), 95–104. 10.1016/0021-8502(95)00531-5

Saha PK, Khlystov A, Snyder MG, & Grieshop AP (2018). Characterization of air pollutant concentrations, fleet emission factors, and dispersion near a North Carolina interstate freeway across two seasons. Atmospheric Environment, 177, 143–153. 10.1016/j.atmosenv.2018.01.019

Saha PK, Sengupta S, Adams P, Robinson AL, & Presto AA (2020). Spatial correlation of ultrafine particle number and fine particle mass at urban scales: Implications for health assessment. Environmental Science & Technology, 54(15), 9295–9304. 10.1021/acs.est.0c02763 [PubMed: 32603094]

Samaras ZC, Andersson J, Bergmann A, Hausberger S, Toumasatos Z, Keskinen J, Haisch C, Kontses A, Ntziachristos LD, Landl L, Mamakos A, & Bainschab M (2020). Measuring automotive exhaust particles down to 10 nm. SAE Technical Paper No. 2020-01-2209) 10.4271/2020-01-2209.

Samaras Z, Ntziachristos L, Thompson N, Hallb D, Westerholm R, & Boulterd P (2005). Characterisation of exhaust particulate emissions from road vehicles. European Commission Contract No. 2000-RD.11091). PARTICULATES Program https://trimis.ec.europa.eu/project/characterisation-exhaust-particulate-emissions-road-vehicles.

Samet JM, Graff D, Berntsen J, Ghio AJ, Huang Y-CT, & Devlin RB (2007). A comparison of studies on the effects of controlled exposure to fine, coarse and ultrafine ambient particulate matter from a single location. Inhalation Toxicology, 19(Suppl 1), 29–32. 10.1080/08958370701492706 [PubMed: 17886047]

Sasaki S (2002). Measurement of Particle Size Distribution of Vehicle Exhaust - how can we reproduce the vehicular PM size in the atmosphere in a laboratory test?. In Proceedings of the CRC workshop on vehicle exhaust particulate emission measurement methodology (San Diego, CA).

Schmid O, & Stoeger T (2016). Surface area is the biologically most effective dose metric for acute nanoparticle toxicity in the lung. Journal of Aerosol Science, 99, 133–143. 10.1016/j.jaerosci.2015.12.006

Schraufnagel DE (2020). The health effects of ultrafine particles. Experimental & Molecular Medicine, 52(3), 311–317. 10.1038/s12276-020-0403-3 [PubMed: 32203102]

Seinfeld JH, & Pandis SN (2016). Atmospheric chemistry and physics: From air pollution to climate change. John Wiley & Sons.

Shanty F (1974). Respiratory deposition of ultrafine particles. Baltimore, MD, USA: [Doctoral Thesis, Johns Hopkins University.

Shi JP, & Harrison RM (1999). Investigation of ultrafine particle formation during diesel exhaust dilution. Environmental Science & Technology, 33(21), 3730–3736. 10.1021/es981187l

Shi JP, Mark D, & Harrison RM (2000). Characterization of particles from a current technology heavy-duty diesel engine. Environmental Science & Technology, 34 (5), 748–755. 10.1021/es990530z

Sierra Instruments. (n.d.). Sierra instruments partial flow dilution (PFD) system. Last accessed on 9/23/2020 at https://www.sierrainstruments.com/autotest/products/emissions-analytical/bg3.html.

Solomon PA (2012). An overview of ultrafine particles in ambient air. Equipment Management: Air and Waste Management Association's Magazine for Environmental Managers, 18–27.

Sturm PJ, Baltensperger U, Bacher M, Lechner B, Hausberger S, Heiden B, Imhof D, Weingartner E, Prevot ASH, Kurtenbach R, & Wiesen P (2003). Roadside measurements of particulate matter size distribution. Atmospheric Environment, 37(37), 5273–5281. 10.1016/j.atmosenv.2003.05.006

Su C, Hampel R, Franck U, Wiedensohler A, Cyrys J, Pan X, Wichmann H-E, Peters A, Schneider A, & Breitner S (2015). Assessing responses of cardiovascular mortality to particulate matter

air pollution for pre-, during- and post-2008 Olympics periods. Environmental Research, 142, 112–122. 10.1016/j.envres.2015.06.025 [PubMed: 26133808]

Tatli E, & Clark N (2008). Crankcase particulate emissions from diesel engines. SAE International Journal of Fuels and Lubricants, 1(1), 1334–1344. 10.4271/2008-01-1751

Testo. (n.d.). Testo DiSCmini handheld nanoparticle counter. Retrieved March 2, 2021 https://www.testo.com/en-US/testo-discmini/p/133.

Todea AM, Beckmann S, Kaminski H, Bard D, Bau S, Clavaguera S, Dahmann D, Dozol H, Dziurowitz N, Elihn K, Fierz M, Lidén G, Meyer-Plath A, Monz C, Neumann V, Pelzer J, Simonow BK, Thali P, Tuinman I, … Asbach C (2017). Inter-comparison of personal monitors for nanoparticles exposure at workplaces and in the environment. The Science of the Total Environment, 605, 929–945. [PubMed: 28688352]

TSI. (n.d.a). Cascade impactors. Retrieved March 2, 2021 https://tsi.com/products/cascade-impactors/.

TSI. (n.d., b). Particle size spectrometers. Retrieved March 2, 2021 https://tsi.com/products/particle-sizers/particle-size-spectrometers/.

TSI. (n.d., c). Ultrafine particle monitor. Retrieved March 2, 2021 https://www.tsi.com/discontinued-products/ultrafine-particle-monitor-3031/.

U.S. CFR. (2018a). United States code of federal regulations. Title 40, Part 50, Appendix L. Last accessed on 3/20/2018 at https://www.ecfr.gov.

U.S. CFR. (2018b). United States code of federal regulations. Title 40, Part 1065, §1065.101, §1065.140, and §1065.240. Last accessed on 3/20/2018 at https://www.ecfr.gov.

U.S. CFR. (2018c). United States code of federal regulations. Title 40, Part 1065, Subpart J. Last accessed on 3/20/2018 at https://www.ecfr.gov.

U.S. CFR. (2020a). United States code of federal regulations. Title 40, Part 50, §50.6. Last accessed on 9/3/2020 at https://www.ecfr.gov/.

U.S. CFR. (2020b). United States code of federal regulations. Title 40, Part 50, §50.7. Last accessed on 9/3/2020 at https://www.ecfr.gov/.

U.S. EPA. (n.d.). Air Quality System (AQS). Retrieved November 2021. https://www.epa.gov/aqs/.

U.S. EPA. (2004). Air quality criteria for particulate matter (EPA Document No. EPA 600/P-99/002aF-bF). U.S. Environmental Protection Agency.

U.S. EPA. (2009). Integrated science assessment (ISA) for particulate matter (EPA Document No. EPA/600/R-08/139F). U.S. Environmental Protection Agency.

U.S. EPA. (2011). Policy assessment for the review of the particulate matter national ambient air quality standards (EPA Document No. EPA 452/R-11-003). U.S. Environmental Protection Agency.

U.S. EPA. (2019). Integrated science assessment (ISA) for particulate matters (EPA Document No. EPA 600/R-19/188). U.S. Environmental Protection Agency.

U.S. EPA. (2020). National emissions inventory (NEI) data. U.S. Environmental Protection Agency. https://www.epa.gov/air-emissions-inventories/2017-national-emissions-inventory-nei-data.

U.S. EPA. (2021). Clean trucks plan regulatory impact analysis (Chapter 3).2. Publication pending.

Uy D, Storey J, Sluder CS, Barone T, Lewis S, & Jagner M (2016). Effects of oil formulation, oil separator, and engine speed and load on the particle size, chemistry, and morphology of diesel crankcase aerosols. SAE International Journal of Fuels and Lubricants, 9(1), 224–238.

Vaaraslahti K, Virtanen A, Ristimäki J, & Keskinen J (2004). Nucleation mode formation in heavy-duty diesel exhaust with and without a particulate filter. Environmental Science & Technology, 38(18), 4884–4890. 10.1021/es0353255 [PubMed: 15487800]

Vander Wal RL, Ticich TM, & Stephens AB (1999). Can soot primary particle size be determined using laser-induced incandescence? Combustion and Flame, 116 (1–2), 291–296.

Vander Wal RL, & Weiland KJ (1994). Laser-induced incandescence: Development and characterization towards a measurement of soot-volume fraction. Applied Physics B, 59(4), 445–452.

Vanhanen J, Mikkilä J, Lehtipalo K, Sipilä M, Manninen HE, Siivola E, Petäjä T, & Kulmala M (2011). Particle size magnifier for nano-CN detection. Aerosol Science and Technology, 45(4), 533–542. 10.1080/02786826.2010.547889

Vogt R, Scheer V, Casati R, & Benter T (2003). On-road measurement of particle emission in the exhaust plume of a diesel passenger car. Environmental Science & Technology, 37(18), 4070–4076. 10.1021/es0300315 [PubMed: 14524437]

Wei Q, Kittelson DB, & Watts WF (2001). Single-stage dilution tunnel performance, SAE technical paper No. 2001-01–0201. SAE International. 10.4271/2001-01-0201

Whitby KT (1967). Aerosol research at the university of Minnesota. Journal of the Air Pollution Control Association, 17(9), 576–578. [PubMed: 6077558]

Whitby KT, Clark WE, Marple VA, Sverdrup GM, Sem GJ, Willeke K, Liu BYH, & Pui DYH (1975). Characterization of California aerosols—I. Size distributions of freeway aerosol. Atmospheric Environment, 9(5), 463–482.

Whitby KT, Husar RB, & Liu BYH (1972). The aerosol size distribution of Los Angeles smog. Journal of Colloid and Interface Science, 39(1), 177–204.

Whitby KT, & Sverdrup GM (1980). California aerosols: Their physical and chemical characteristics. In Hidy GM, Mueller PK, & Grosjean D (Eds.), The character and origins of smog aerosols: A digest of results from the California aerosol characterization experiment (ACHEX) (pp. 478–517). Wiley.

Willeke K, & Whitby KT (1975). Atmospheric aerosols: Size distribution interpretation. Journal of the Air Pollution Control Association, 25(5), 529–534.

Wilson WE, Stanek J, Han H-SR, Johnson T, Sakurai H, Pui DYH, Turner J, Chen D-R, & Duthie S (2007). Use of the electrical aerosol detector as an indicator of the surface area of fine particles deposited in the lung. Journal of the Air & Waste Management Association, 57(2), 211–220. 10.1080/10473289.2007.10465321 [PubMed: 17355082]

Yokoi T, Shinzawa M, & Matsumoto Y (2001). Measurement repeatability improvement for particle number size distributions from diesel engines. JSAE Review, 22 (4), 545–551. 10.1016/S0389-4304(01)00136-9

Zhang S, & McMahon W (2012). Particulate emissions for LEV II light-duty gasoline direct injection vehicles. SAE Int. J. Fuels Lubr, 5(2), 637–646. 10.4271/2012-01-0442

Zhang KM, & Wexler AS (2004). Evolution of particle number distribution near roadways—Part I: Analysis of aerosol dynamics and its implications for engine emission measurement. Atmospheric Environment, 38(38), 6643–6653. 10.1016/j.atmosenv.2004.06.043

Zhang KM, Wexler AS, Zhu YF, Hinds WC, & Sioutas C (2004). Evolution of particle number distribution near roadways. Part II: The ‘Road-to-Ambient’ process. Atmospheric Environment, 38(38), 6655–6665. 10.1016/j.atmosenv.2004.06.044

Zhu Y, Hinds WC, Kim S, Shen S, & Sioutas C (2002b). Study of ultrafine particles near a major highway with heavy-duty diesel traffic. Atmospheric Environment, 36(27), 4323–4335. 10.1016/S1352-2310(02)00354-0

Zhu Y, Hinds WC, Kim S, & Sioutas C (2002a). Concentration and size distribution of ultrafine particles near a major highway. Journal of the Air & Waste Management Association, 52(9), 1032–1042. 10.1080/10473289.2002.10470842 [PubMed: 12269664]

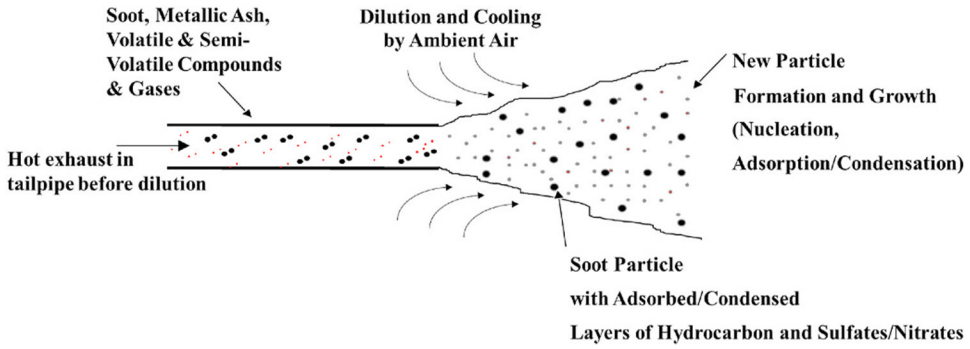

Figs. 2–1.

A schematic representation of engine exhaust particle formation during dilution and cooling with ambient air illustrating gaseous, semi-volatile, and solid (nonvolatile) constituents.

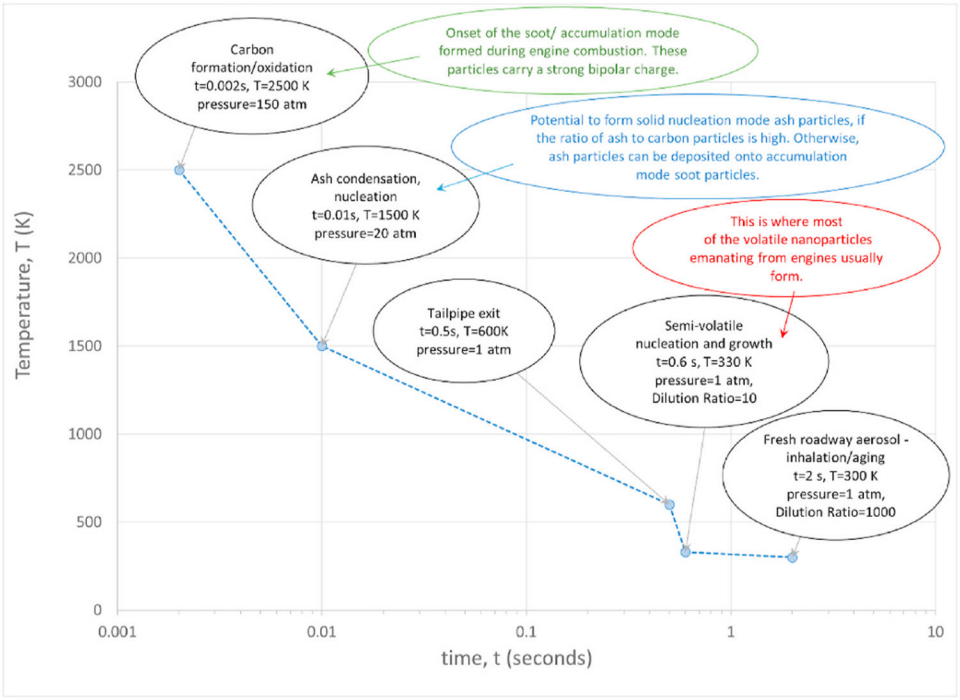

Fig. 2–2.

Particle formation history of a near-roadway diesel aerosol. Adapted from (Kittelson 2006a).

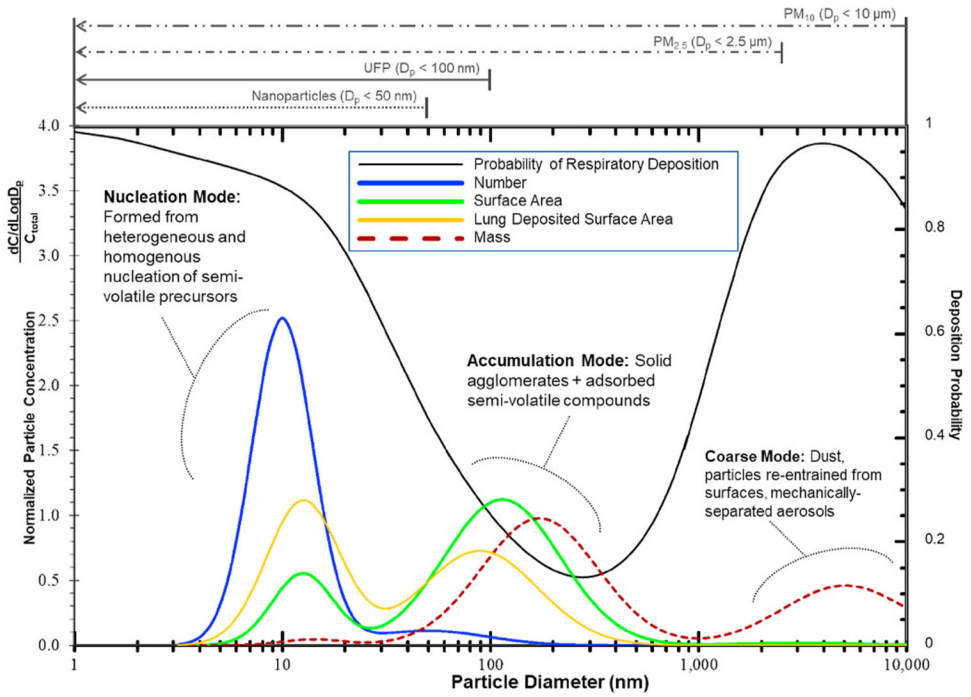

Figs. 2–3.

Comparison of particle size distributions for different metrics of number, surface area, lung deposited surface area, and mass. Adapted from Kittelson (1998) and Kittelson and Kraft (2015) with further addition of lung deposited surface area size distribution. The integrated areas (C_{total}) under the number, mass, LDSA and area size-distributions are proportional to the total number, surface area, and mass concentrations and are the normalization factors. The black line near the top of the figure shows the probability of respiratory deposition for comparison. Respiratory deposition is based upon the ICRP model adapted from Maynard and Kuempel and from Oberdörster et al. (International Commission on Radiological Protection, 1994; Maynard & Kuempel, 2005; Oberdörster et al., 2007). Modeled conditions were light exercise with nasal breathing at 25 L/min. Particles were modeled as spherical with a density of 1 g/cm^3.

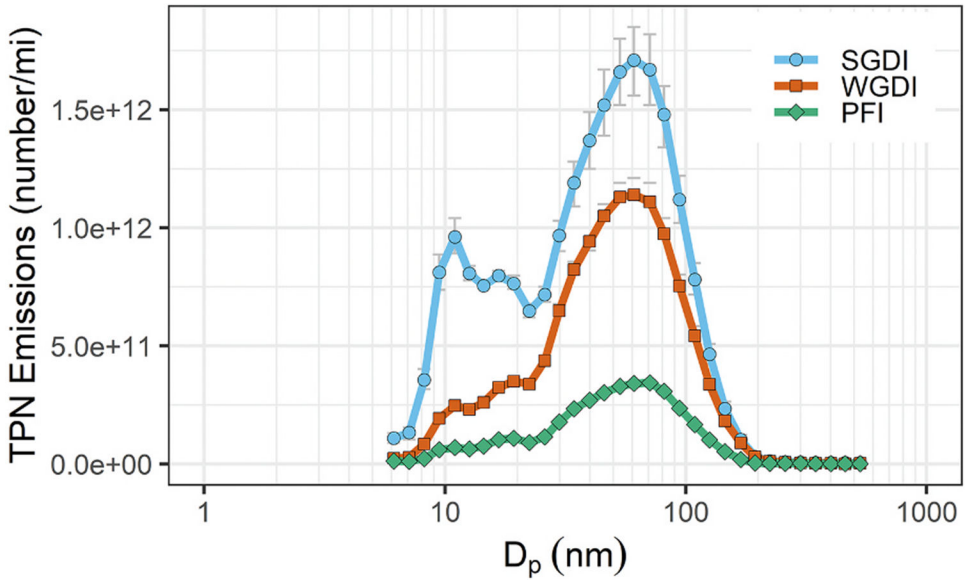

Figs. 2–4.

Number weighted size distributions produced by three types of gasoline SI engines: spray guided direct injection (SGDI), wall guided spray direct injection (WGDI) and port fuel injection (PFI).

Adapted with permission (Zhang & McMahon, 2012)

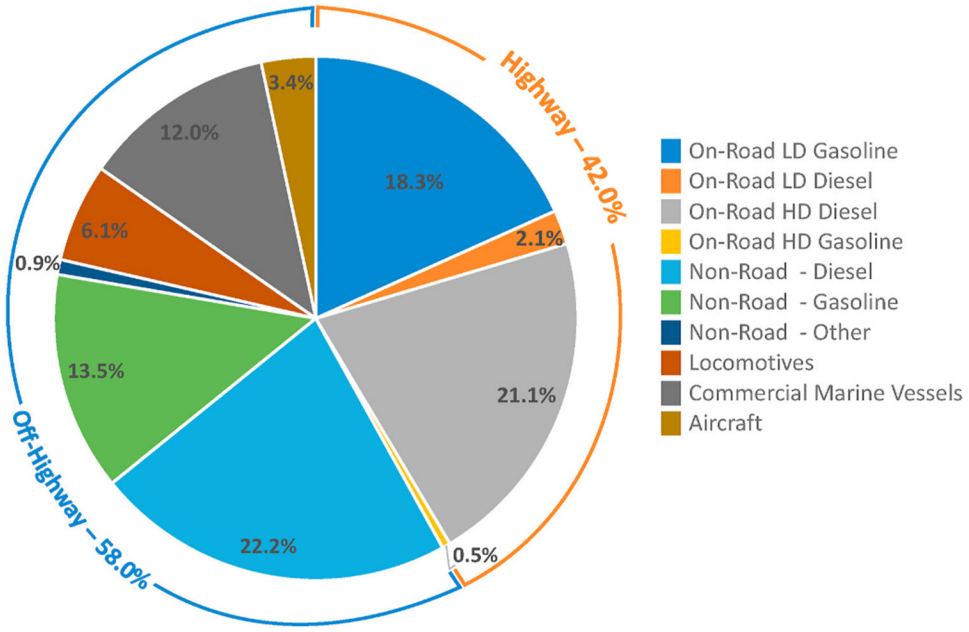

Figs. 3–1.

Relative contribution of major highway and off-highway categories to direct emissions of fine particles ($PM_{2.5}$) from mobile sources in the United States based on EPA 2017 National Emissions Inventory (NEI) Data. Mobile sources account for approximately 20% of anthropogenic fine particle emissions in the U.S (U.S. EPA, 2020, p. 2017).

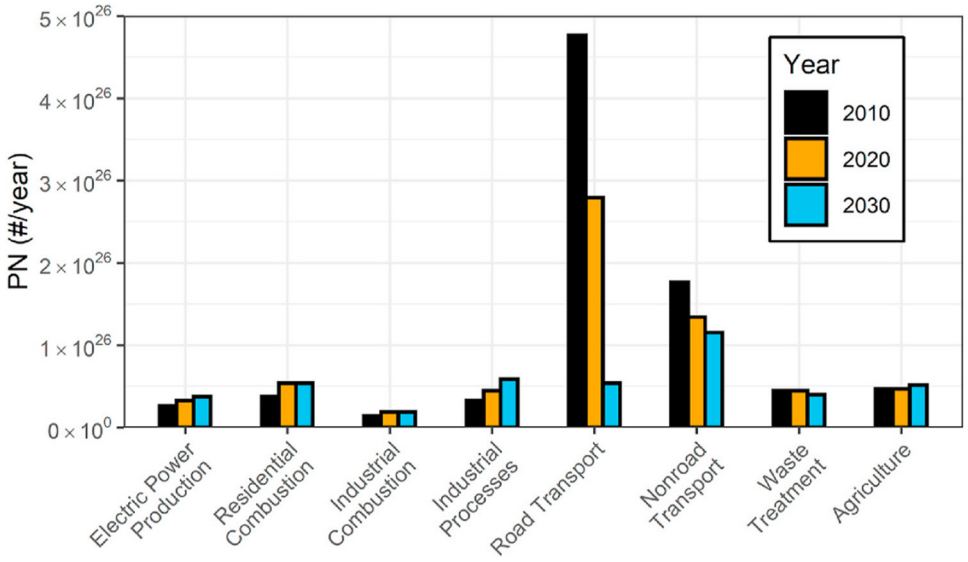

Figs. 3–2.

GAINS modeling results of the contributions of different source sectors to total particle number emissions in North America for 2010, 2020, and 2030.

Adapted from Paasonen et al. (2016).

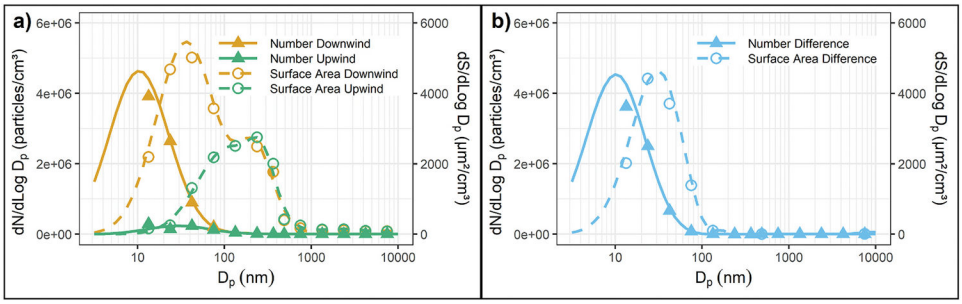

Figs. 4–1.

Particle size distributions measured upwind and downwind of an urban freeway (adapted from Whitby et al., 1975). (a) Shows measured upwind and downwind particle surface area and number concentrations. (b) Shows difference between upwind and downwind size distributions, i, e., particles added by the traffic. All lines shown are based on bimodal lognormal fits.

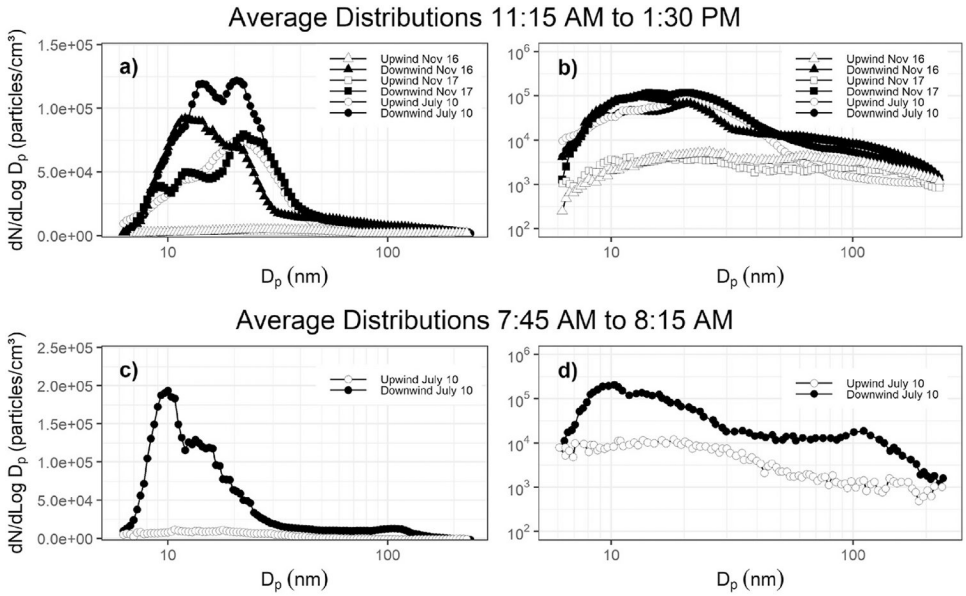

Figs. 4–2.

Roadside particle size distributions upwind and downwind of a California freeway. adapted from Nanzetta and Holmén (2004).

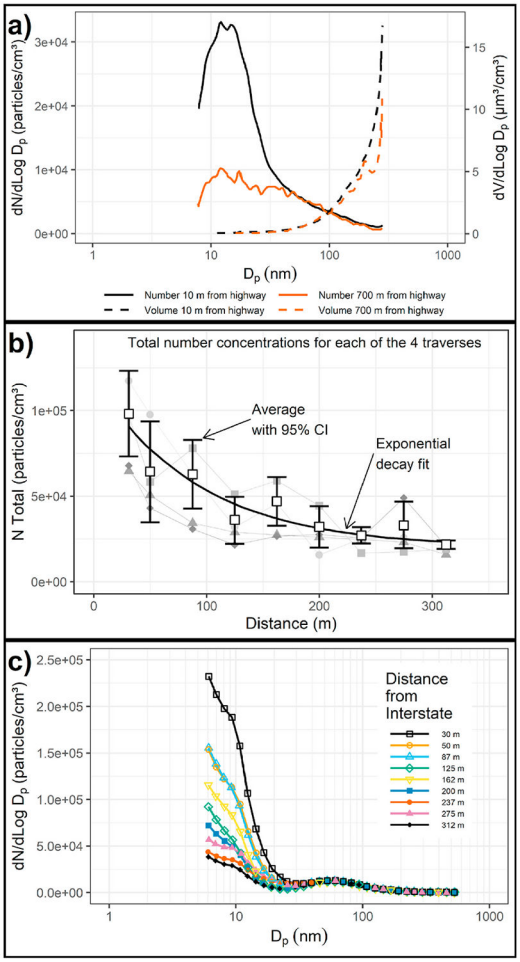

Figs. 4–3.

(a) Size distribution measurements made 10 m and 700 m from an urban freeway in Minnesota. Adapted from Kittelson, Watts, and Johnson (2004). (b) Particle number concentrations measured in traverses perpendicular to an interstate highway. Adapted from Jacobson et al. (2005). Panel C: Particle number weighted size distributions measured in traverses perpendicular to an interstate highway.

Adapted from Jacobson et al. (2005).

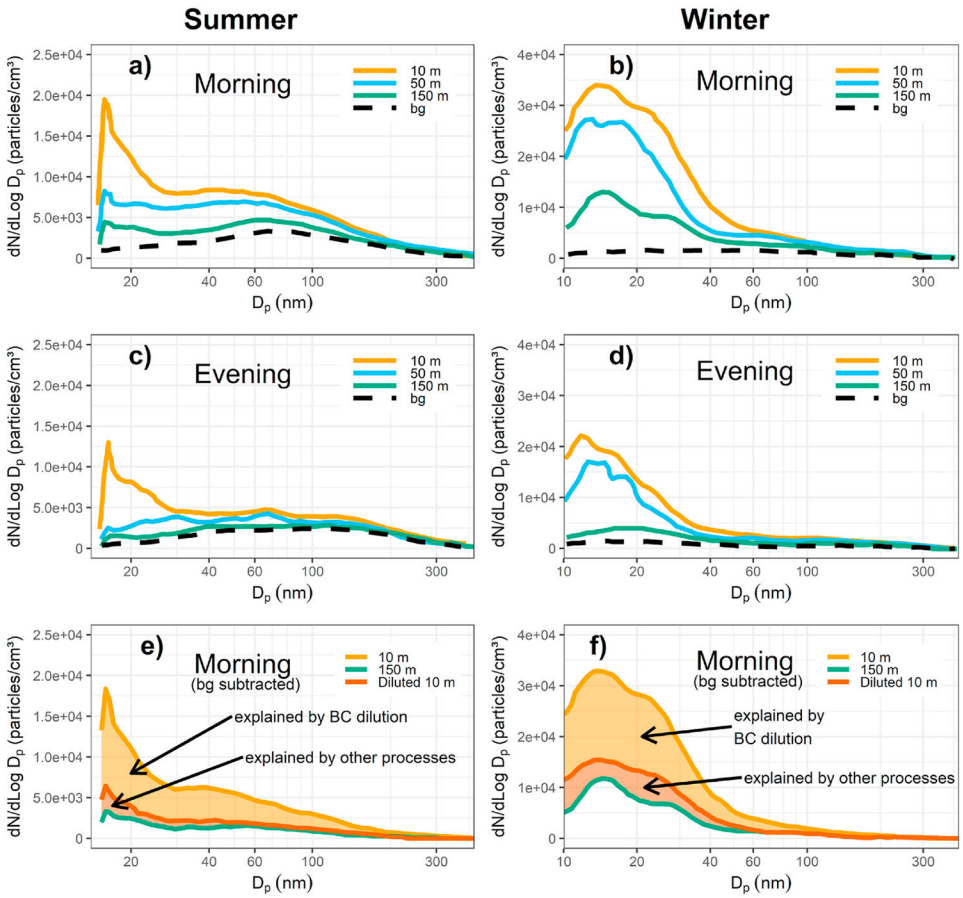

Fig. 4–4.

(a–d) Average particle number size distributions at different distances from the roadway edge. Downwind measurements are not background-subtracted. (e–f) Background-subtracted average particle number size distributions at 10 m (red) and 150 m (purple) downwind distances. Figure adapted from (Saha et al., 2018).

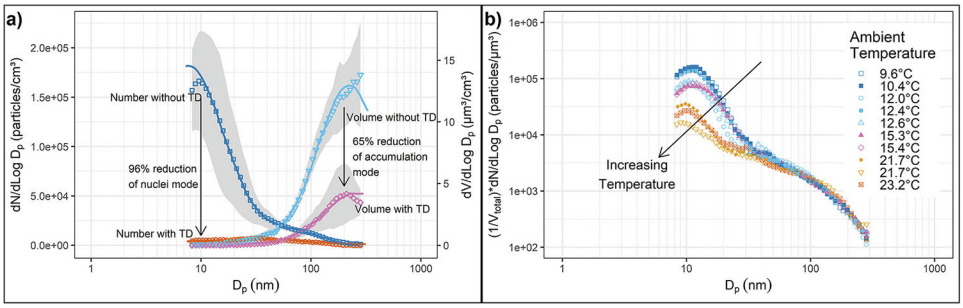

Figs. 4–5.

(a) Average size distributions measured during 60 h of testing in truck traffic on a New York State freeway. Results are shown with and without a thermal denuder that removes semi-volatile particles. (b) Normalized particle size distributions measured during 60 h of testing in truck traffic on a New York State freeway. They have been normalized to give a constant number concentration in the accumulation mode so that the relative size of the nucleation and accumulation mode can be seen. Results are shown for an ambient temperature range from 9.6 to 23.2 C.

Adapted from Kittelson, Watts, Johnson, et al. (2004).

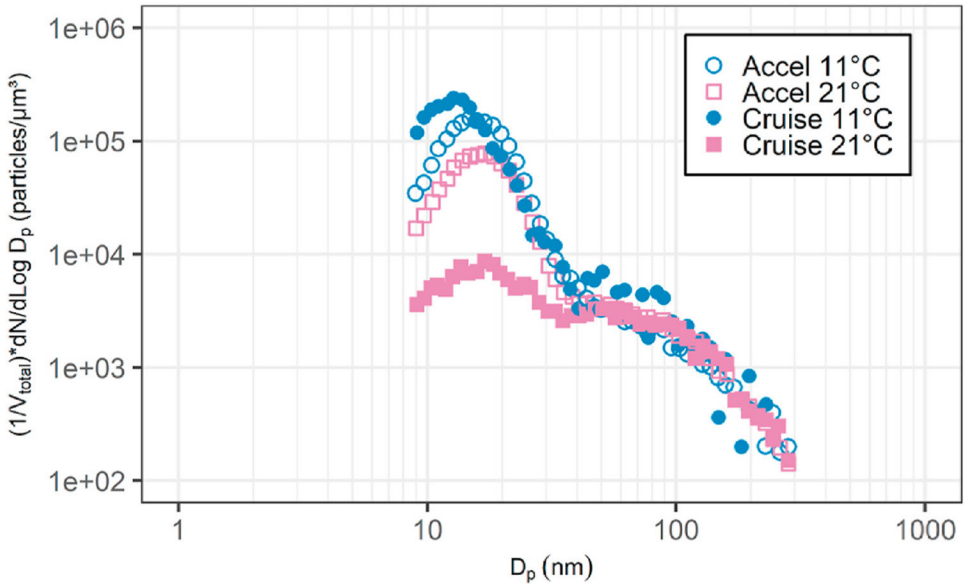

Figs. 4–6.

Size distributions measured in on-road chase experiments on two consecutive days with different ambient temperatures. The truck from which the emissions were being measured was powered by Cummins ISM engine running low sulfur reformulated California fuel (S < 100 ppm). Results are corrected for background aerosols and normalized to a unit volume concentration of 1 $\mu m^3/cm.^3$.

Adapted from Kittelson et al. (2000).

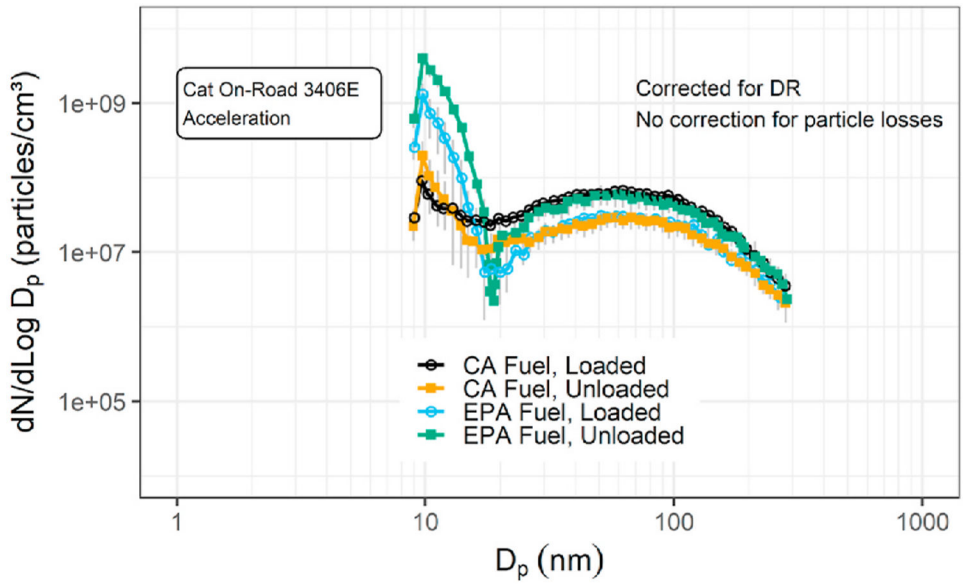

Figs. 4–7.

Size distributions measured in on-road chase experiments. Source truck powered by Caterpillar 3406E engine. Acceleration experiments with loaded and unloaded truck, California fuel (S < 100 ppm S) and U.S. fuel (S = 350 ppm). Corrected for background and dilution ratio.

Adapted from Kittelson et al. (2002).

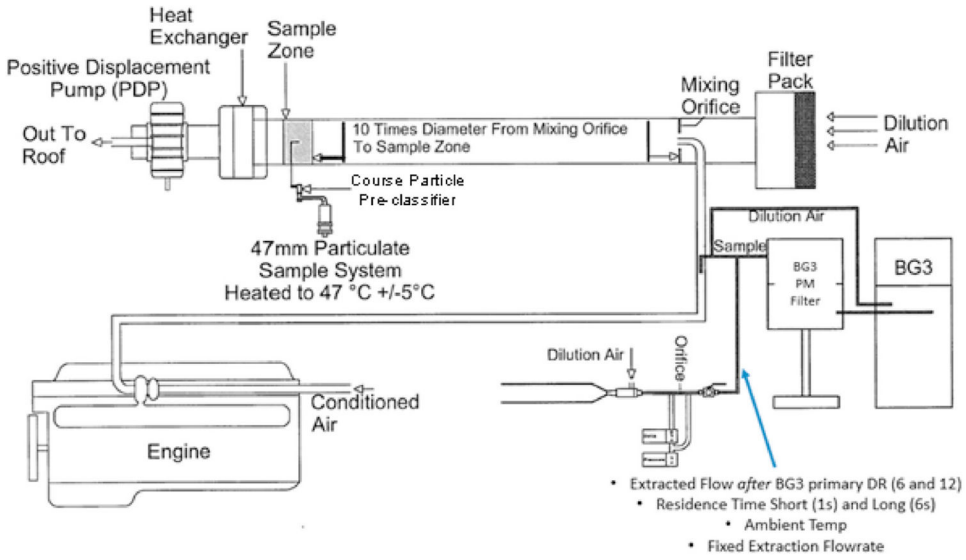

Figs. 4–8.

An example of a full and partial flow sampling, BG3 partial flow dilution (.Sierra Instruments. (n.d.)) system.

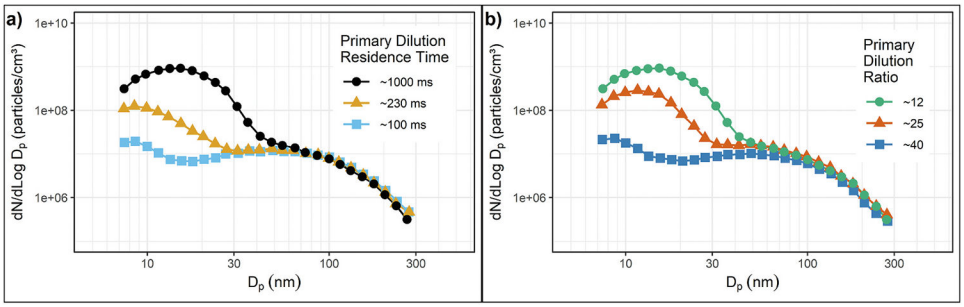

Figs. 4–9.

(a) The effect of primary dilution residence time (PRT) on nanoparticle emissions. (b) The effect of primary dilution ratio (PDR) on nanoparticle formation.

Adapted with permission (Khalek et al., 1999).

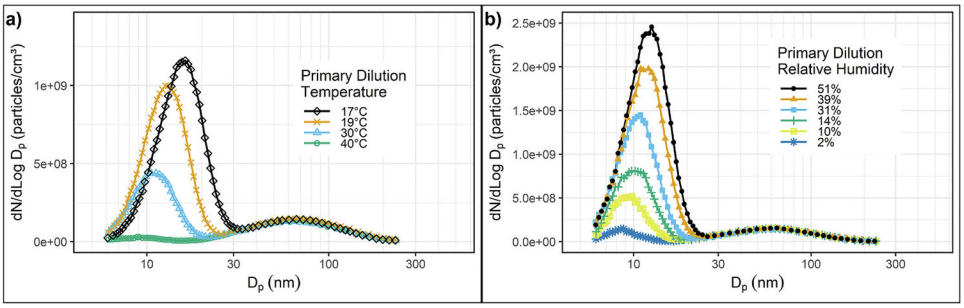

Figs. 4–10.

(a) Influence of primary dilution temperature (PDT) on nanoparticle formation. (b) Influence of relative humidity on nanoparticle formation.

Adapted with permission (Mathis et al., 2004).

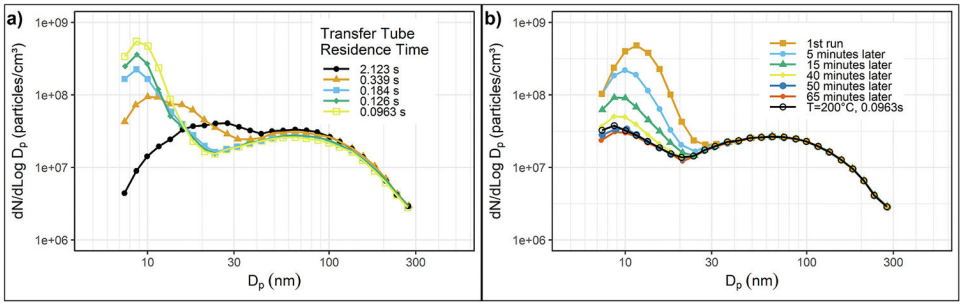

Figs. 4–11.

(a) The effect of Sample Transfer Tube Residence Time on Nanoparticle Emissions for uncatalyzed diesel exhaust. (b) Evolution of exhaust size distributions after raising transfer line temperature from 200 to 305 °C.

Adapted with permission (Wei et al., 2001).

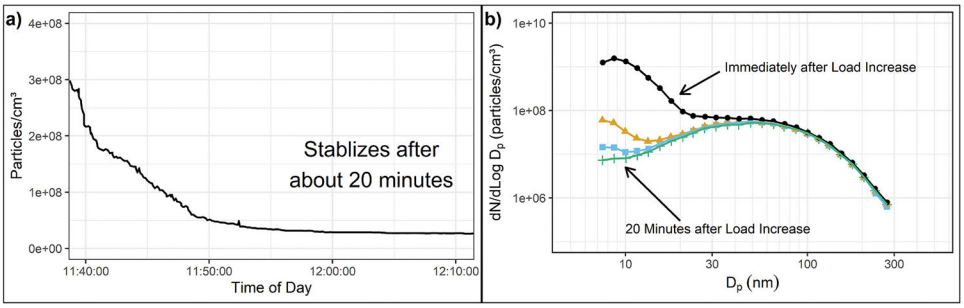

Figs. 4–12.

(a) Transient measurements of total particle number concentration in diesel engine exhaust measured with a CPC after transition from a stabilized idle condition to rated power @ 2600 rpm. (b) Particle size distributions measured with SMPS after transition from a stabilized idle condition to rated power @2600 rpm and measured at 5–6 min intervals after the transition.

Adapted with permission (Kittelson & Khalek, 1999).

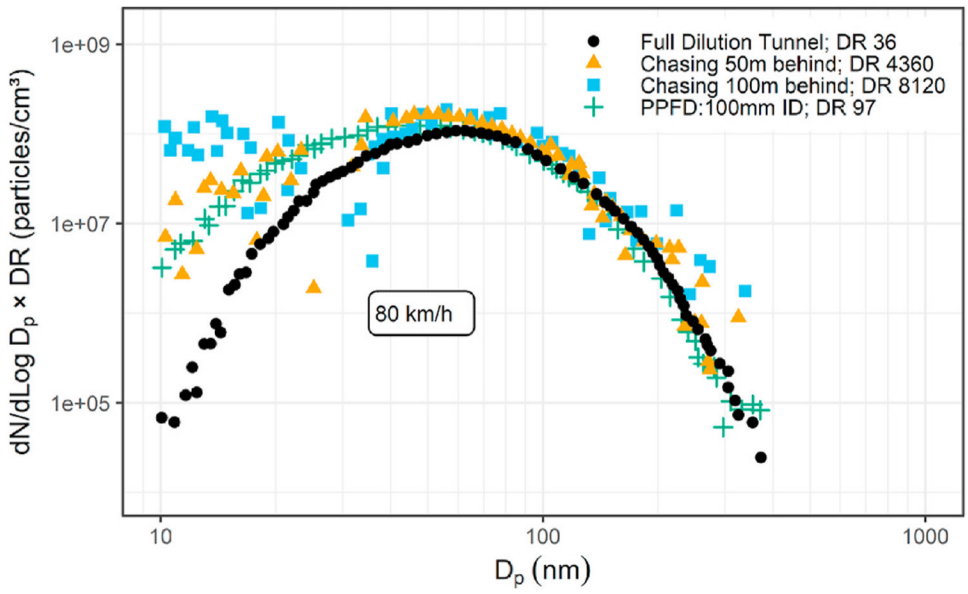

Figs. 4–13.

Comparison of chase experiment and partial flow dilution.

Adapted with permission (Sasaki, 2002).

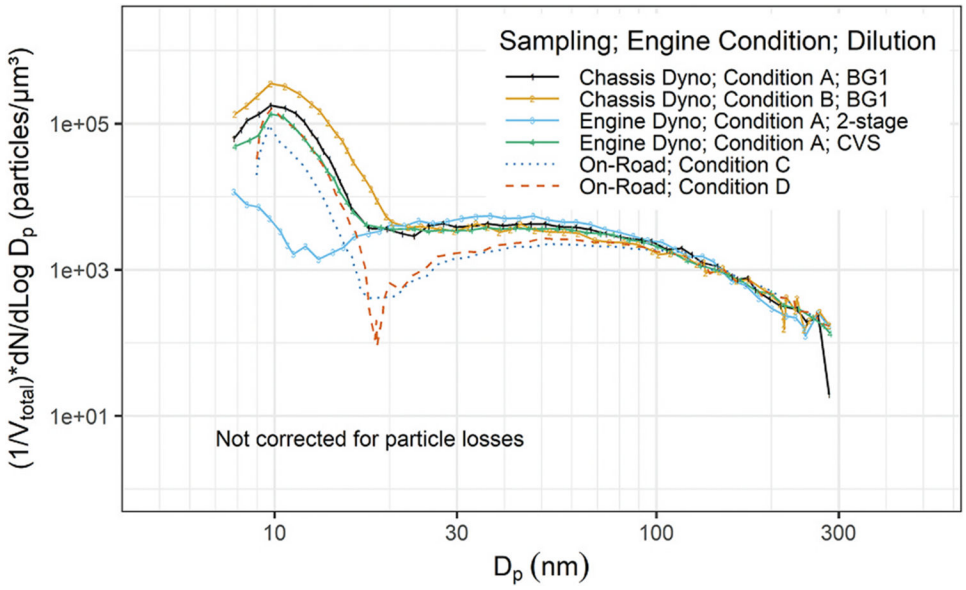

Figs. 4–14.

Comparison of size distribution measured under on-road chase conditions and with various laboratory dilution schemes: CVS denotes CVS tunnel followed by ejector dilutor, BG1 denotes BG-1 porous tube dilutor followed by ejector dilutor, 2-stage denotes two stage ejector dilutor Condition A:1800 rpm, 2250 N m; Condition B: 1610 rpm, 2012 N·m; Condition C: on-road acceleration with loaded trailer; Condition D: on-road acceleration with unloaded trailer. Condition A and B intended to mimic conditions C and D, respectively.

Adapted from Kittelson et al., 2002.

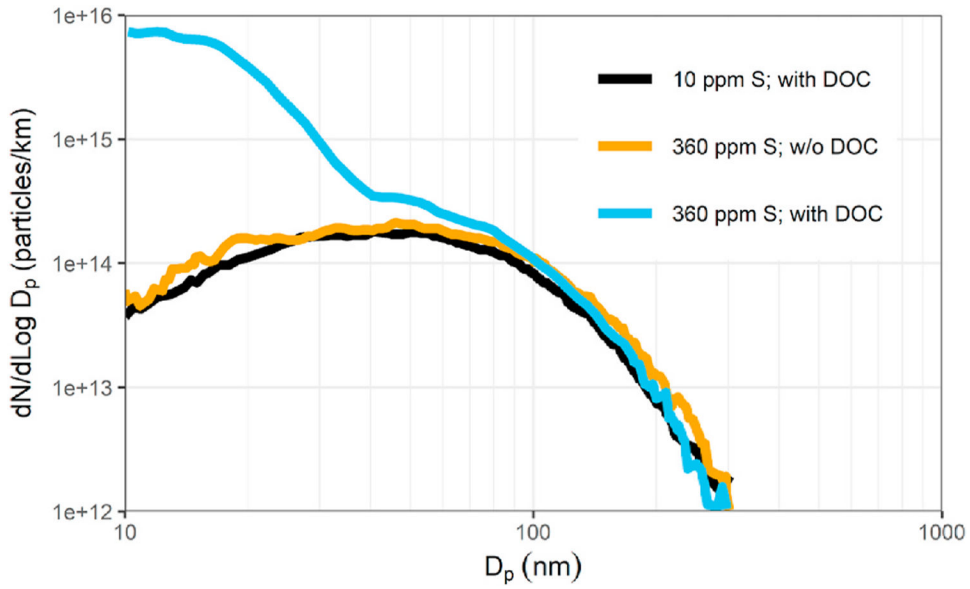

Figs. 4–15.

On-road size distributions measured in the plume of a Euro 3 diesel passenger car with and without a diesel oxidation catalyst (DOC). adapted from Vogt et al. (2003).

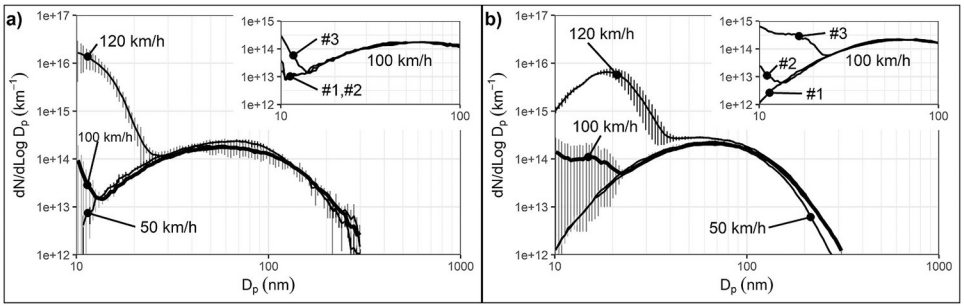

Figs. 4–16.

Particle size distributions obtained at different speeds during: (a) Vehicle chasing and (b) laboratory measurements. The inset in each panel shows the development of the nucleation mode over time at 100 km/h for three consecutive SMPS scans.

Adapted from Giechaskiel et al. (2005).

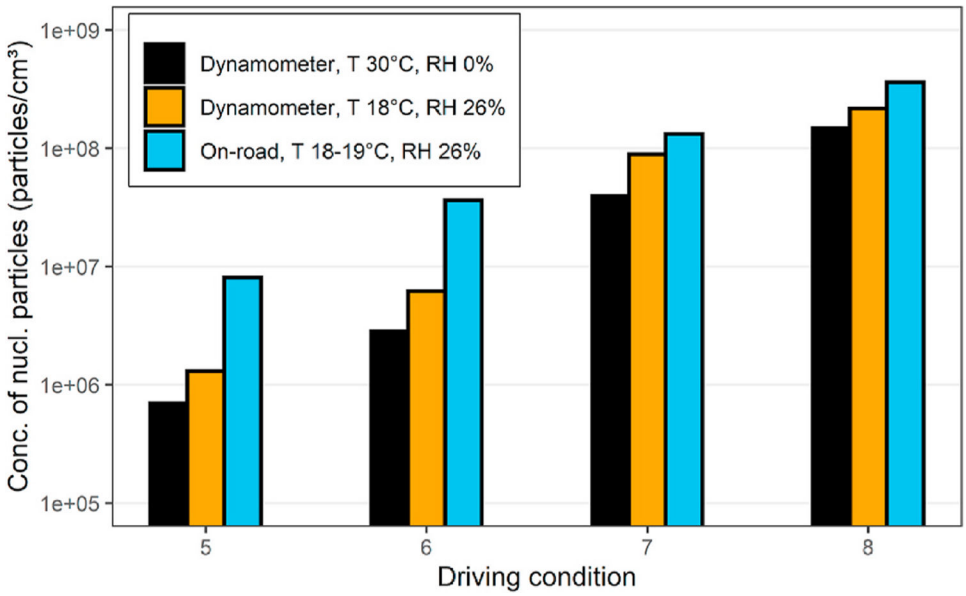

Figs. 4–17.

Comparison of nucleation mode concentrations measured on-road and in the laboratory for a Euro III bus operating at 40 kph adapted from Rönkkö et al. (2006).

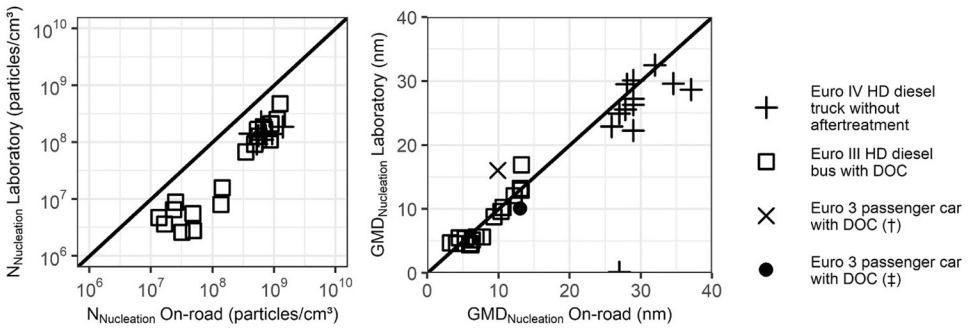

Figs. 4–18.

Comparison of laboratory and on-road measurements of nucleation mode concentration and size adapted from Keskinen and Rönkkö (2010).

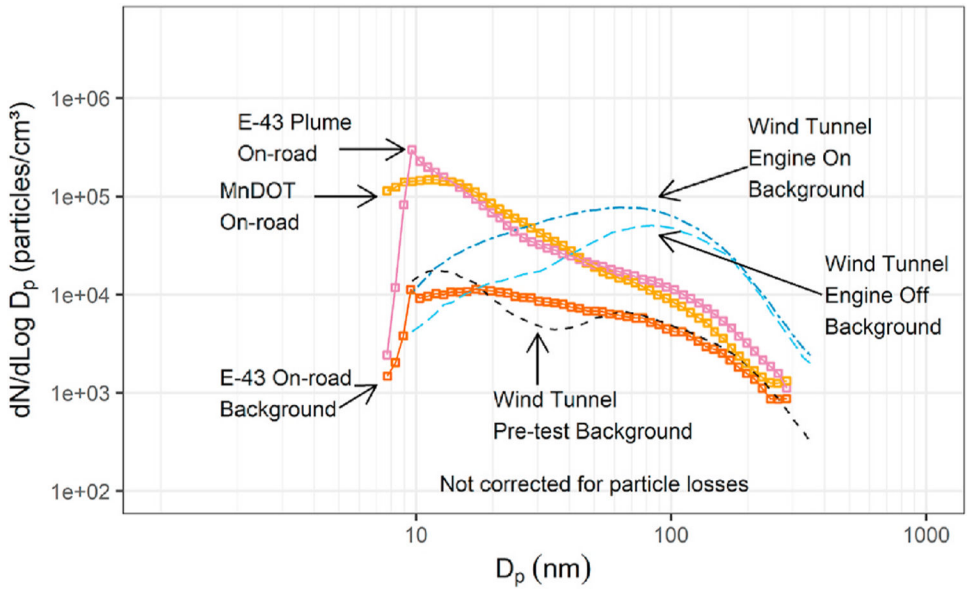

Figs. 4–19.

Wind tunnel, on-road size, and near road size distribution measurements. Adapted with permission (Kittelson et al., 2000).

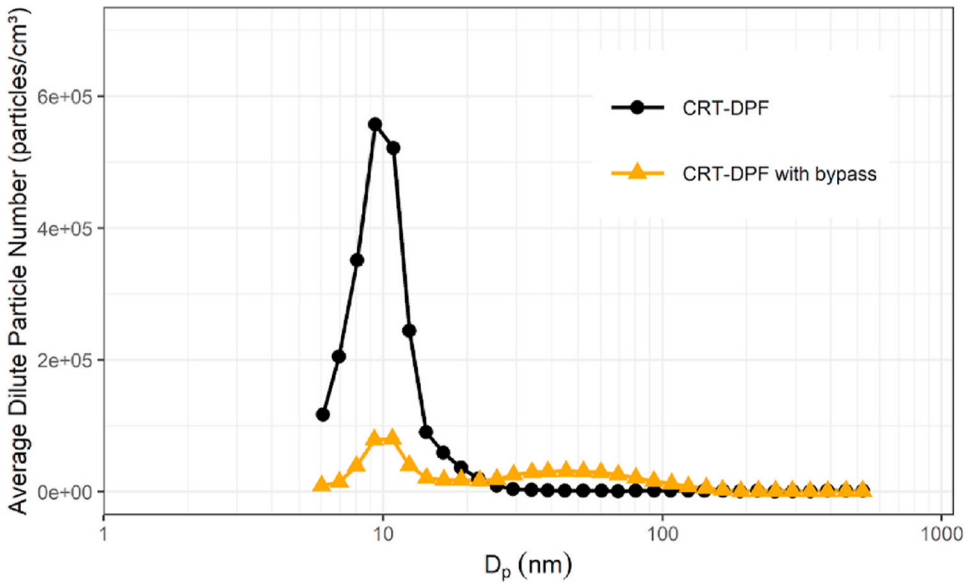

Figs. 4–20.

Nanoparticle formation in the presence and absence of soot particles. Adapted with permission (Khalek, 2006a).

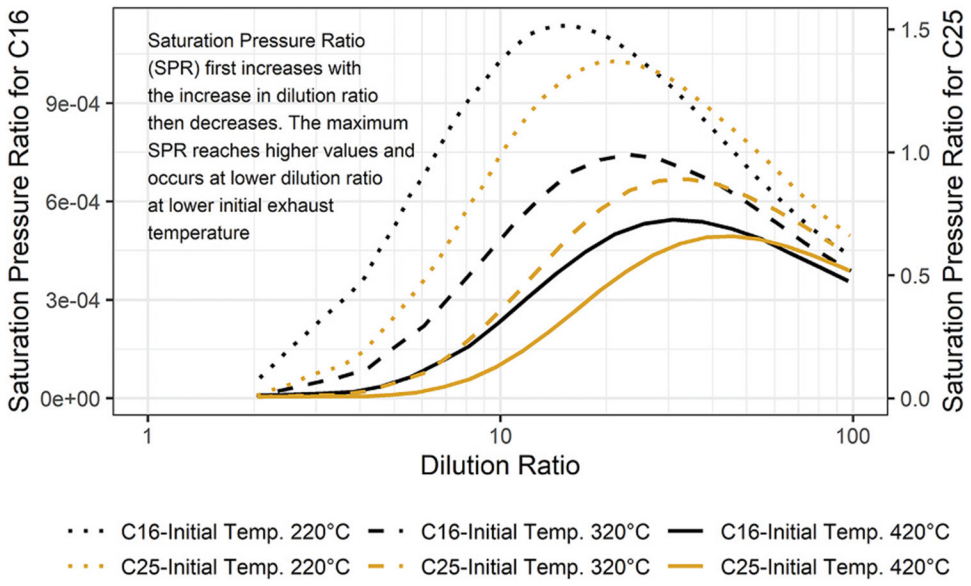

Figs. 4–21.

Saturation Pressure ratio for C16 and C25 as a function of dilution ratio (dilution air at 25 °C) for different exhaust temperatures Adapted with permission from Khalek (2006b, p. 2).

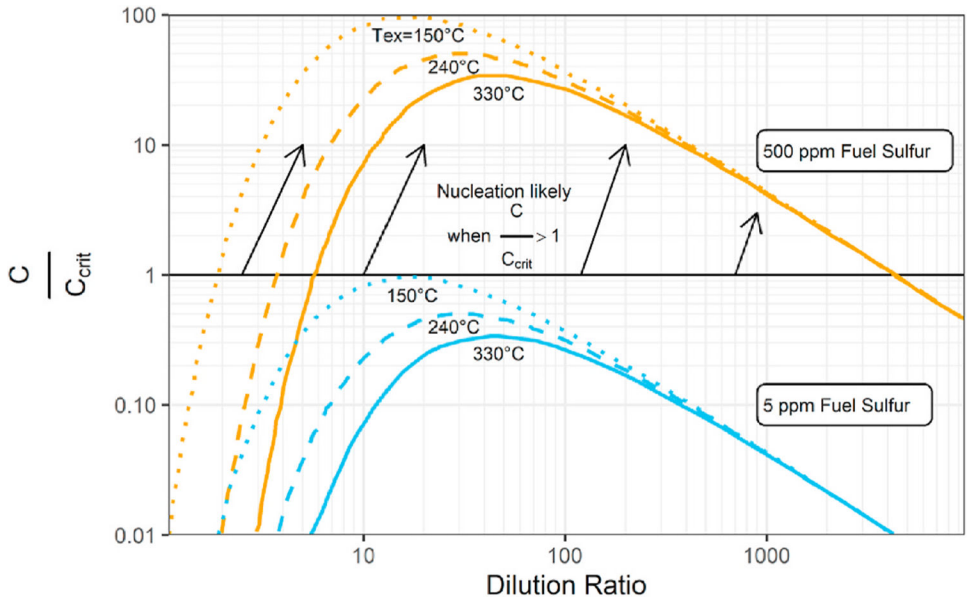

Figs. 4–22.

Ratio of actual sulfuric acid concentration to the concentration necessary to trigger binary sulfuric acid/water nucleation. Ratios for 500 ppm fuel sulfur are shown in orange and ratios for 5 ppm fuel sulfur are shown in blue. Ambient temperature and relative humidity 27 °C and 40%, engine air-fuel ratio = 30. Exhaust initially particle free. Critical concentration calculated using model from Seinfeld and Pandis and (2016).

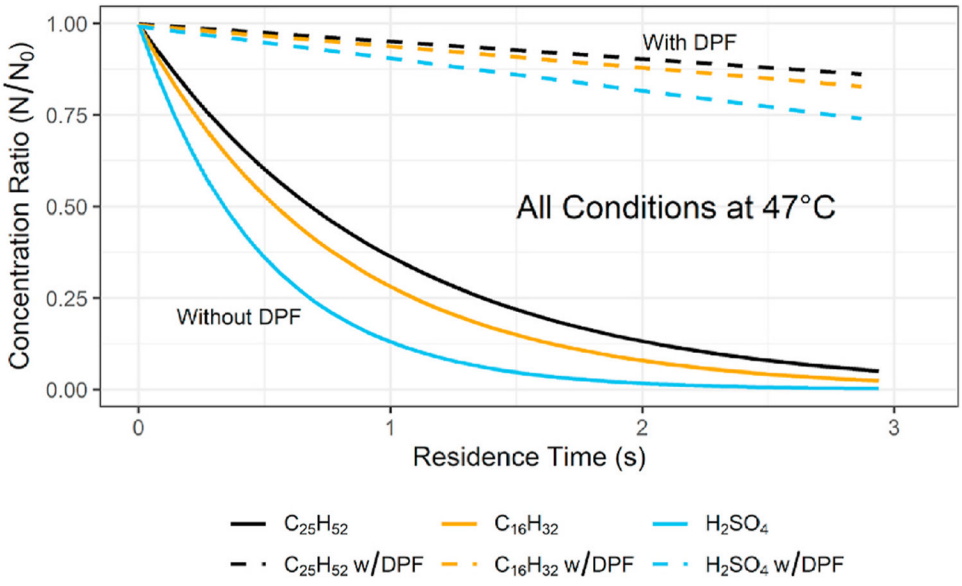

Figs. 4–23.

Volatile and Semi-volatile decay due to adsorption on soot particles with a sticking coefficient of 1 using high soot concentration (Without DPF) and low soot concentration (with DPF). Adapted with permission from Khalek (2006b, p. 2).

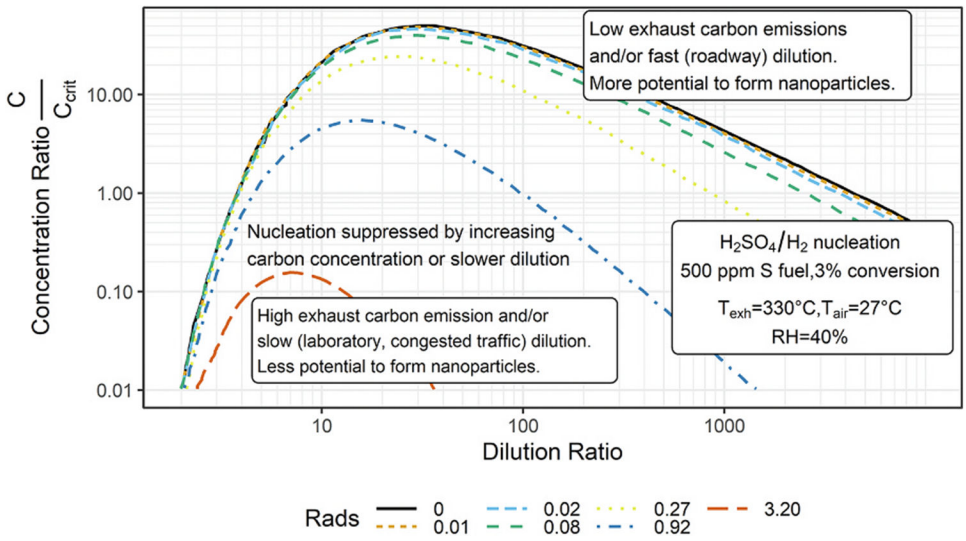

Figs. 4–24.

Ratio of actual sulfuric acid concentration to the concentration necessary to trigger binary sulfuric acid/water nucleation. Ambient temperature and relative humidity 27 °C and 40%, engine air-fuel ratio = 30, sulfuric acid concentration in exhaust = 15 ppm. Particles present in exhaust adsorb sulfuric acid and suppress nucleation, Rads = (Rate of adsorption to surface of particles present in exhaust)/(Rate of dilution). Critical concentration calculated using model from Seinfeld and Pandis (2016).

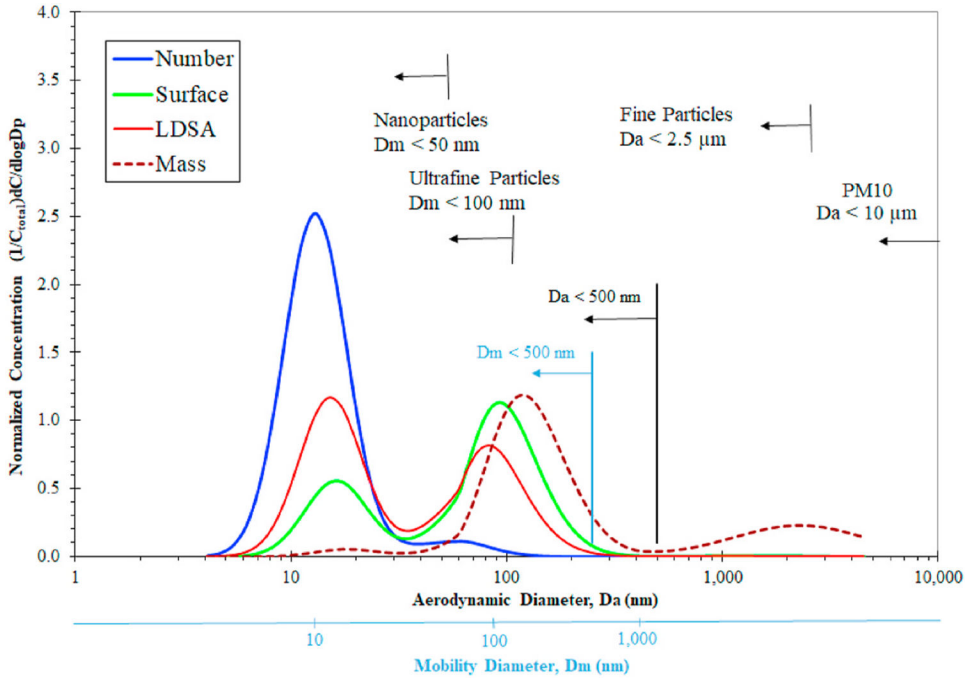

Figs. 5–1.

Combustion particle number, surface area, LDSA and mass distribution as a function of (a) mobility diameter (Dm) and (b) aerodynamic diameter (Da).

Tables 4–1

Influence of sampling system design on measured concentration of nucleation mode particles.

Investigator	Dilution system	Increase PDT	Increase RT	Increase PDR	Increase PRH	Comments
Khalek et al. (1999)	ED (dry/humid) + AC + ED (dry)	Strong decrease	Strong increase (Figs. 4–9a)	Decreasing to constant above PDR = 60 (Figs. 4–9b)	Modest increase	
Shi et al. (1999)	CVS (humid) + ED (dry)			Increase with CVS primary dilution,	Increase	Multiple test campaigns with same engine, highly variable results
Shi et al. (2000)	ED (dry) + ED (dry)			Decrease with ED primary dilution	Increase	Same as above
Mathis et al. (2004)	PRD (humid) + AC + ED (dry)	Strong decrease (Figs. 4–10a)	Increase in size, decrease in concentration	Peak at intermediate PDR = 23	Strong increase (Figs. 4–10b)	Stable and repeatable results
Lyyränen et al. (2004)	Heated * PRD(dry)+ED or Heated ED (dry) + ED	PRD 200 °C ED 182 °C slight increase for ED		Small mode insensitive to conditions		Both PRD and ED first stage dilution gave similar results
	PFD (dry) + ED (dry)			Increase in PDR range 2.5–5.3		
	PRD (dry) single stage			No NM, decrease in AM to constant above DR ~50		

Abbreviations: NM – nucleation mode, AM – accumulation mode, ED – ejector dilutor, AC – aging chamber, CVS – constant volume sampler (dilution tunnel), PFD – partial flow dilutor, PRD – porous tube dilutor, PDT – temperature in first (primary) dilution stage, RT – residence time in aging chamber, PDR – primary dilution ratio, PRH – primary dilution relative humidity.

Secondary dilution, when used, was mainly to “freeze” the aging process by reducing concentrations but did not significantly change the shape of the size distributions.

* They used heated dilution to remove or prevent formation of semi-volatile particles giving stable results but not predictive of atmospheric dilution.

Tables 5–1

Summary of recommended metric definitions.

Single Metric UFP[a]	**Continuous Size Distribution Based UFP**[d]
~3 nm ≤ UFP-N ≤ 500 nm[b]	~3 nm ≤ UFP-N ≤ 500 nm[b]
UFP-S[c] ≤ 500 nm (Use of 500 nm Inertial Separator)	UFP-S[c] ≤ 500 nm
UFP-M ≤ 500 nm (Use of 500 nm Inertial Separator)	UFP-M ≤ 500 nm

N: Number, S: Surface, M: Mass.

[a] Upper limit set by inertial classification; lower limit set by instrument limitation.

[b] As stated in the text, most UFP-N is below 100 nm; inertial seprator not needed.

[c] Surface area or Lung deposited surface area, UFP-LDSA.

[d] Upper and lower size boundaries imposed by instrument limitations and/or applied by postprocessing.